Proximity labelling reveals the compartmental proteome of murine sensory neurons

Julia R Sondermann[1]*, Allison M Barry[1]*, Feng Xian[1], Thomas Haberl[1], David Gomez-Varela[1], Fritz Benseler[2], Dietmar Schreiner[3], Noa Lipstein[2,4], Nils Brose[2], Manuela Schmidt[1λ]

1. Systems Biology of Pain, Division of Pharmacology & Toxicology, Department of Pharmaceutical Sciences, University of Vienna, Austria
2. Department of Molecular Neurobiology, Max Planck Institute for Multidisciplinary Sciences, 37075 Göttingen, Germany
3. Biozentrum, University of Basel, Basel, Switzerland
4. Leibniz-Forschungsinstitut für Molekulare Pharmakologie (FMP), 13125 Berlin, Germany

** these authors contributed equally*

[λ] corresponding author: Manuela Schmidt; manuela_schmidt@univie.ac.at

Keywords

sensory neuron; proximity labelling; TurboID; DIA-MS; CIPN; DRG; bulk proteomics

Abstract

Understanding the molecular architecture of peripheral sensory neurons is critical as we pursue novel drug targets against pain and neuropathy. Sensory neurons in the dorsal root ganglion (DRG) show extensive compartmentalization, thus understanding each compartment – from the peripheral to central terminals – is key to this effort. To systematically profile this spatial complexity, we generated a TurboID$^{fl/fl}$ transgenic mouse line (ROSA26$^{em1(TurboID)Bros}$), enabling targeted proximity labelling and deep proteomic profiling of DRG neuron compartments via Advillin^{Cre}. Our data reveal distinct proteomic signatures across neuronal compartments that reflect specialized neuronal functions. We provide proteomic insights into previously inaccessible nerve terminals both in the periphery (innervating the skin) and in the spinal cord. Further, using a DRG explant model of chemotherapy-induced peripheral neuropathy (CIPN), we uncovered novel and discrete proteome changes, highlighting neuronal vulnerability. Together, our findings provide a unique proteome atlas of the sensory neuron proteome across anatomical domains and demonstrate the utility of proximity labelling proteomics for detecting compartment-specific molecular alterations in a disease model. This dataset serves as a valuable resource for mechanistic studies of sensory neuron function and pathology.

Introduction

Dorsal root ganglia (DRG) serve as critical hubs in the peripheral nervous system (PNS), housing the somata of sensory neurons that transmit information from the periphery to the central nervous system (CNS).[1] DRG comprise sensory neurons as well as other cells, including glial and immune cells that provide essential support for neuronal function and are implicated in PNS pathologies. Consequently, the interpretation of bulk proteomics data from DRG is inherently complex and requires downstream validation to discern cell type-specific changes.

Adding to this complexity, sensory neurons exhibit remarkable spatial compartmentalization. Understanding the spatial proteome of sensory neurons and its dynamics is critical for elucidating the molecular mechanisms underlying sensory processing, neuronal maintenance, and pathological conditions such as chronic pain. Somata are located far from their target organs and afferent synapses in the CNS, connected via axons that can extend up to more than a meter in length. Obtaining a comprehensive, cell-type- and compartment-specific proteomic profile of DRG neurons remains a significant technical challenge. Although techniques like fluorescence-activated cell sorting (FACS) can isolate specific cell types, they prioritize somata and/or nuclei. Isolating intact subcellular compartments, particularly the peripheral terminals/"free nerve endings", as well as the axons of sensory neurons remains a major hurdle.

In recent years, proximity-dependent labelling techniques combined with mass spectrometry (MS), such as TurboID-based biotinylation-dependent labelling and APEX, have emerged as powerful tools for mapping subcellular proteomes and interactomes in living cells and tissues.[2,3] TurboID is an engineered, promiscuous biotin ligase that enables rapid and efficient labelling of proteins within a 9–10 nm radius in living cells.[4] To date, most applications of TurboID and its predecessor BioID have involved fusion proteins with compartment-specific targeting sequences, enabling selective biotinylation of proximal interactomes for downstream affinity purification and identification via MS.[5–7]

Unlike TurboID fusion proteins, the use of soluble TurboID variants enables unbiased labelling of the entire accessible proteome within a cell, providing a comprehensive snapshot of its proteomic composition. Sunna et al. demonstrated that TurboID-mediated biotinylation covers approximately 59–65% of the proteome in neuroblastoma (N2A) and microglia (BV2) cell lines expressing a cytosolic TurboID variant.[8] By comparing the biotinylated proteome of these two cell lines, they revealed cell-type-specific proteome differences and captured proteome dynamics in response to an inflammatory challenge *in vitro*.

To explore cell-type-specific *in vivo* protein biotinylation and identification, Rayaprolu et al. developed an adenoviral and transgenic mouse model expressing TurboID in distinct

cell types, including neurons and astrocytes, across different brain regions, thereby uncovering region-specific proteomic differences in astrocytes.[9] In another *ex vivo* study, Hobson et al. employed APEX2 proximity labelling combined with MS to map the proteomic differences between somatodendritic and axonal compartments in acute brain slices.[10] They demonstrated how the compartmental proteome correlates with respective neuronal functions and identified ion channels with previously unrecognized axonal localization. This provided deeper insights into the molecular architecture of dopaminergic neurons.[10] These findings highlight the potential of proximity-dependent labelling approaches for mapping the proteome of spatially complex structures such as DRG neurons.

Here, we applied TurboID-based proximity labelling *in vivo* using a Cre-lox system. Paired to an Advillin^{Cre} driver[11], this restricts TurboID expression to DRG sensory neurons. We were able to systematically profile the proteomes of distinct neuronal compartments, including somata (lumbar levels 3-5 DRG (L3-L5)), central synaptic terminals (terminals$_c$) in the dorsal lumbar spinal cord (SC), axons (sciatic nerve; SCN), and peripheral terminals (terminals$_p$) from paw skin, providing the first compartmentalized proteomic atlas of lumbar sensory neurons.

We then harnessed this technique to explore neuronal changes after oxaliplatin treatment in an *in vitro* explant model of chemotherapy-induced peripheral neuropathy (CIPN). CIPN is a common side effect of chemotherapy, with agents damaging sensory neurons and leading to a painful neuropathy often preventing adequate cancer therapy.[12] There are no preventative treatments available to date, thus a deeper understanding is urgently needed. We observed distinct dysregulation across neuronal transporters after oxaliplatin treatment, including some not detected with bulk proteomics. Several of these transporters represent promising candidates for follow-up translational studies.

Together, our findings reveal novel insights into the compartment-specific protein distributions that underlie key aspects of sensory neuron function. Our data also highlight the potential of TurboID-based proteomics to uncover subtle, cell type-specific changes in disease contexts. These datasets serve as valuable resources for future studies on neuronal specialization and pain-related proteomic alterations in the PNS.

Results

We profiled the compartmental proteome of murine sensory neurons using the well characterized Advillin^{Cre} driver[11,13–15] crossed with the here generated TurboID$^{fl/fl}$ (Adv^{Cre};TurboID$^{fl/fl}$) mice (Figure 1). In these transgenic mice, TurboID is expressed in the cytoplasm of Advillin-positive cells, resulting in promiscuous biotinylation of intracellular proteins specifically within sensory neurons. Advillin-negative cells do not express the TurboID ligase and therefore do not label proteins (Fig 1A). We isolated tissue from the spinal cord (SC), dorsal root ganglia (DRG), sciatic nerve (SCN) and paw skin to cover the spatial complexity of DRG sensory neurons, isolating tissue from wildtype mice in parallel (Fig 1B). Biotinylated proteins were enriched after tissue lysis and prior to mass spectrometry, enhancing neuronal protein specificity in comparison to control tissue to account for endogenous biotinylation. Distinct labelling in each tissue of Adv^{Cre};TurboID$^{fl/fl}$ mice was confirmed by immunohistochemistry (Fig 1C, SFig 1A) and validated via Western blotting (SFig 1B).

As expected, we see a clear enrichment of TurboID labelling in sensory neuron terminals in the dorsal root lamina, in neuronal cell bodies in the DRG, axons in the nerve, and nerve endings in the skin (Fig 1C). Using Western blotting, TurboID signal was readily detected in lysates from SC, DRG, and nerve tissues, but less prominent in skin lysates (SFig 1). The latter may be due to low protein quantity after lysis, as TurboID+ afferents are evident by immunohistochemistry (Fig 1C, “skin”).

To generate a comprehensive and quantitative compartmental proteome atlas of DRG neurons, we employed data-independent acquisition combined with parallel accumulation–serial fragmentation (DIA-PASEF) mass spectrometry on Advillin^{Cre} x TurboID (Adv^{Cre};TurboID$^{fl/fl}$) and control tissue (Advillin-negative mice, referred to as TurboID$^{fl/fl}$) (Fig 2, SFig 2-5, STables 1-10). Both overlapping and unique proteins were detected across all 4 DRG compartments (Fig 2A). A comparison of Adv^{Cre};TurboID$^{fl/fl}$ samples with TurboID$^{fl/fl}$ control shows more protein (SFig 2A), more protein groups (SFig 2B), and clustering by condition and compartment (SFig 2C-D). Adv^{Cre};TurboID$^{fl/fl}$ samples cluster by compartment (Fig 2B), and show extensive ion channel coverage, including Trpv1 and Scn10a in the peripheral terminals (Fig 2C). These data highlight the sensitivity and depth of our profiling approach. A full expression matrix is available in STable 1.

Neuronal compartment proteome

In Adv^{Cre};TurboID$^{fl/fl}$ samples proteins were considered enriched based on two criteria: A: proteins detected in Adv^{Cre};TurboID$^{fl/fl}$ samples, but not in TurboID$^{fl/fl}$ samples, or B: proteins significantly upregulated in Adv^{Cre};TurboID$^{fl/fl}$ samples compared to TurboID$^{fl/fl}$ ($\log_2$ fold change (LFC) > 1, FDR < 0.05, using a moderated T-Test through limma) (Fig 2D, STable 2). These upregulated proteins are referred to as differentially expressed

proteins (DEPs). The enriched proteins were then combined, and treated equally for all downstream analyses.

We identified the highest number of enriched proteins in the somata (DRG), followed by the central terminals (terminals$_c$, SC), axons (SCN), and finally the peripheral terminals (terminals$_p$, skin), with overlapping and unique proteins (Fig 2E). For each compartment, we see an enrichment of proteins in the Adv^{Cre};TurboID$^{fl/fl}$ sample over TurboID$^{fl/fl}$ (Fig 2F) across the dynamic range (SFig 2E). In addition, there are few negatively correlated proteins, likely reflecting endogenous biotinylation such as in the case of Acaca, Acacb, Mccc1, and Pcca (Fig 2F).[16,17] Together, this results in a curated, compartmental proteome for murine primary sensory neurons ranging from hundreds to thousands of proteins per compartment.

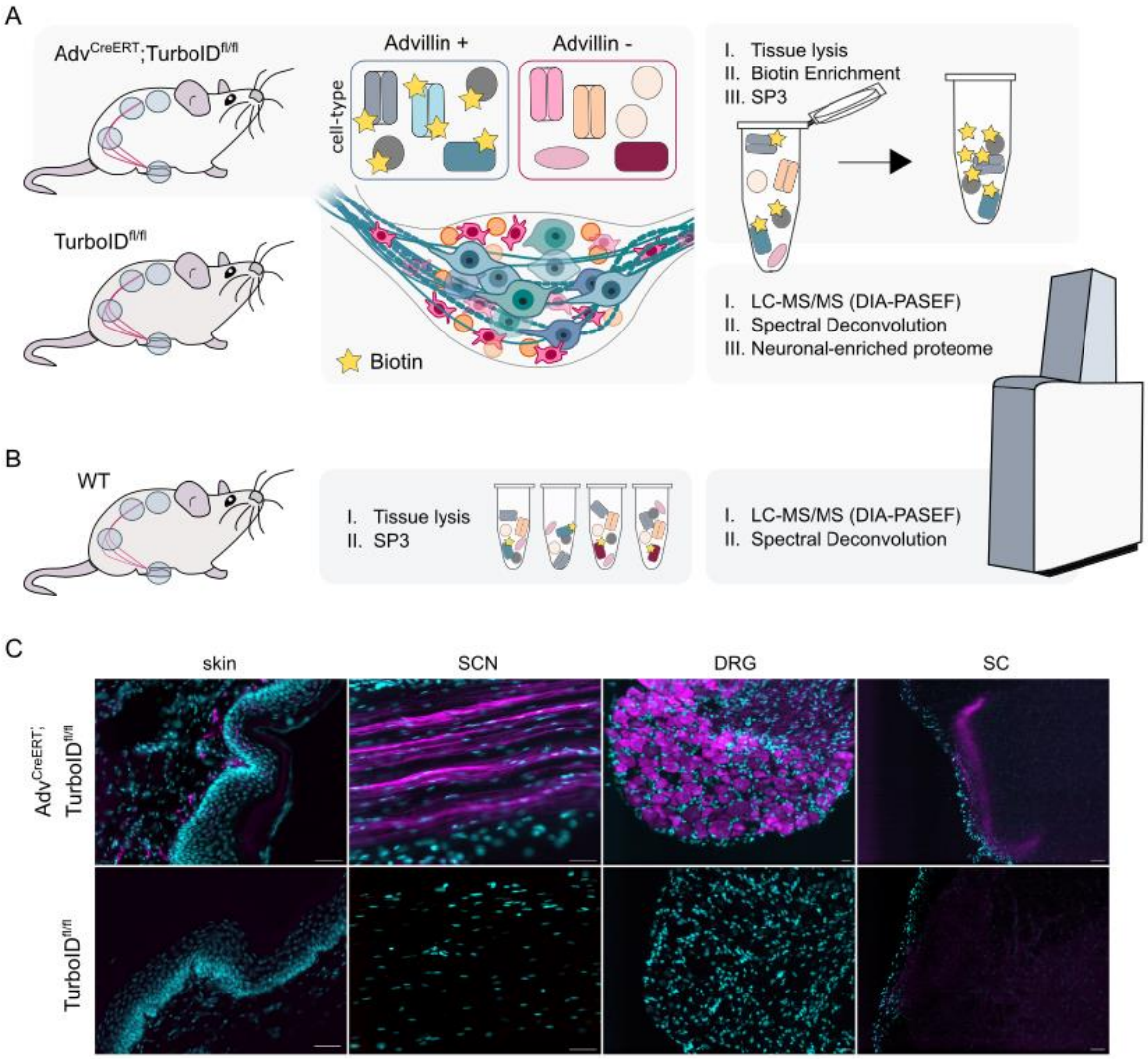

Figure 1. Adv^{Cre};TurboID$^{fl/fl}$ mice were used to target the sensory neuron proteome. A. Schema overview for biotinylation of neuronal proteins. Adv^{Cre};TurboID$^{fl/fl}$ and TurboID$^{fl/fl}$ were provided biotin-enriched water, which, in Adv^{Cre};TurboID$^{fl/fl}$ promote the biotinylation of all proteins within Advillin-expressing (+) cells. Advillin-negative (-) cells only contain endogenously biotinylated proteins. Tissues were lysed, proteins purified for biotin, prior to SP3 and downstream LC-MS/MS via timsTOF HT in DIA-PASEF mode. B. Corresponding bulk proteomes

were isolated from wildtype (WT) mice for each corresponding tissue in A. C. Representative immunohistochemistry from TurboID$^{fl/fl}$ (control) and Adv^{Cre};TurboID$^{fl/fl}$ mice across tissues. Cyan, DAPI. Magenta, Streptavidin-555 (biotin). Scale bar = 50 µm.

Neuronal subtype enrichment

The use of the Advillin^{Cre} transgenic allows targeting the vast majority sensory neurons in the PNS.[13] To evaluate the representation of neuronal subpopulations within our dataset, we performed gene set enrichment analysis using a curated list of subtype markers, described in Barry et al., 2023.[13] As expected, the strongest subtype enrichment was observed in the DRG, with significantly enriched signatures for non-peptidergic and peptidergic nociceptors, as well as a mix of low-threshold mechanoreceptors (LTMRs; include A-field-LTMR, C-LTMR, and AB-LTMR) (Fig 2G). Across all components a positive trend for each subtype emerged. Significant enrichment was particularly notable for non-peptidergic nociceptors, A-field-LTMR, and C-LTMR (Fig 2G, STable 3). These findings indicate that our proximity labelling approach preserves the molecular diversity of sensory neuron subtypes across their anatomical domains.

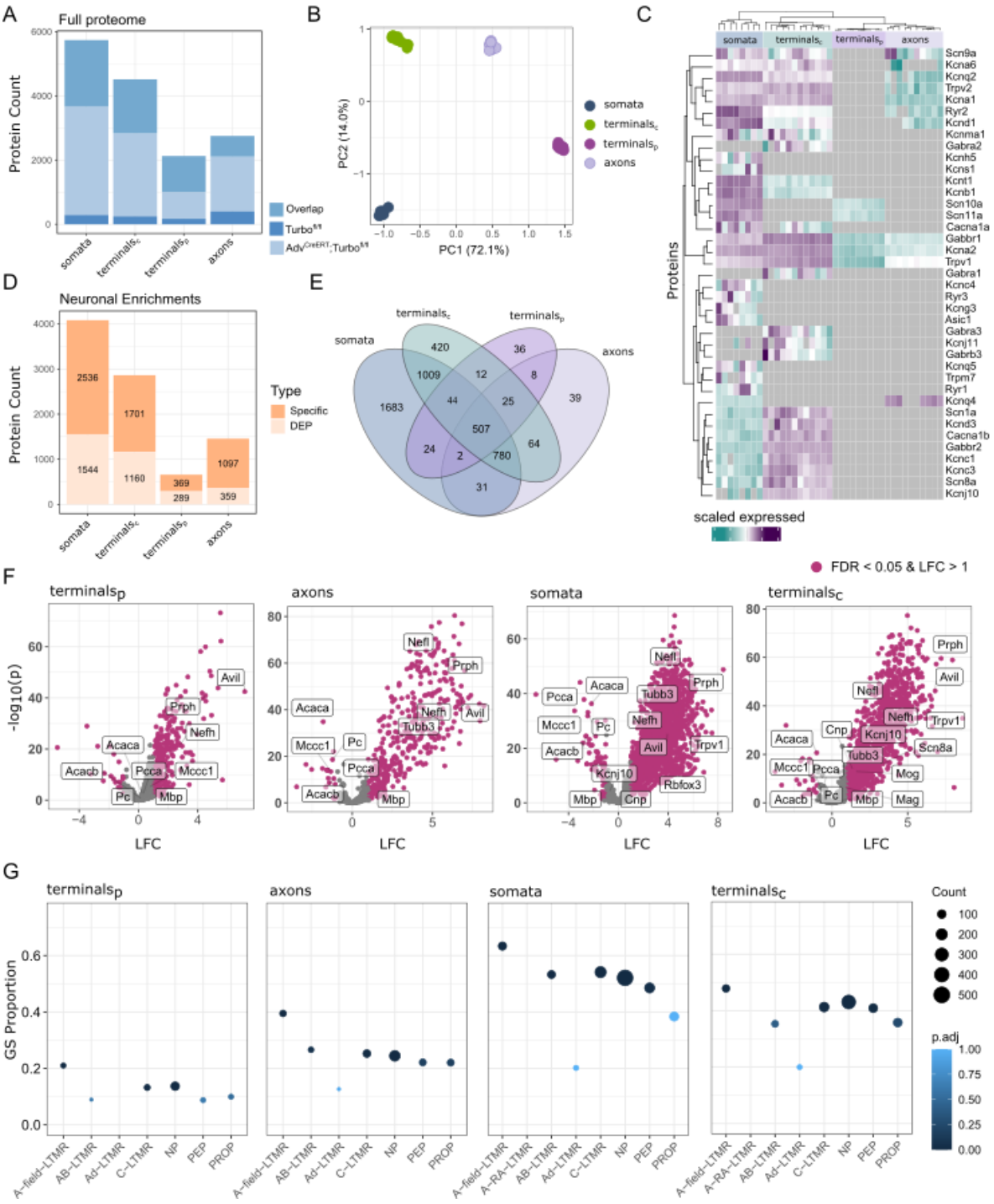

Figure 2. Neuronal proteins are enriched across sensory neuron compartments. A. Protein counts by sample, with "overlap" representing proteins in both Adv^{Cre};TurboID$^{fl/fl}$ and control tissue. B. PCA. C. Heatmap of scaled expression across ion channels in Adv^{Cre};TurboID$^{fl/fl}$ samples. D. Calculated enrichment of neuronal proteins by tissue. E. Comparison of neuronal protein enrichment across tissues. F. Volcano plots highlighted the neuronal enrichment for DEP proteins from D, labelled with neuronal and endogenously biotinylated proteins. G. Gene set enrichment analysis against custom DRG subtype gene lists. Count reflects the number of proteins detected within each gene list, per compartment. GS = gene set. NP = non-peptidergic. PEP = peptidergic. PROP = proprioceptor. LTMR = low threshold mechanoreceptor. LFC = $\log_2$ fold change. terminals$_p$ = peripheral terminals (skin); terminals$_c$ = central terminals (SC).

Compartmental sexual dimorphism

To explore sex-specific molecular differences, we analysed differential protein expression between male and female mice across all compartments (SFig 3). With an FDR < 0.05, the sensory neuron proteome appeared largely conserved between sexes, with a few exceptions in abs(LFC) > 1, such as Lgi1 and Sprr1a in the LSC and Brd4 and Palm2 in the peripheral terminals (SFig 3A, STable 4).

To gain broader biological insights, we also conducted gene set enrichment analysis using ranked LFC. This analysis revealed sexually dimorphic regulation of select pathways (SFig 3B). In the peripheral terminals, we see differences in circulatory and vascular pathways, whereas peptide biosynthesis and macromolecule biosynthesis show differences in the somata. These findings suggest localized sex differences in specific biological processes and highlight pathways of potential interest for future mechanistic studies.

Functional signatures show separation by neuronal compartment

To extract the corresponding functional signature, Gene Ontology (GO) pathway analyses were performed against a background of all proteins expressed in the corresponding tissues (Fig 3). While neuronal signatures are detected in each compartment, they also show functional specificity, as expected (Fig 3, STable 5). Primary afferents synapse on secondary order neurons in the dorsal horn of the spinal cord. This corresponds to the enrichment of proteins involved in presynaptic function and synaptic signalling between neurons, as well as vesicle-mediated transport, exocytosis, and other synapse-related terms in the LSC. The DRG contain neuronal somata, and, thus, corresponding functional enrichment matches expectations. Here, we see the enrichment of proteins involved in mRNA processing, post-translational modification, and nuclear structures, in line with the biosynthetic activity expected in neuronal cell bodies.

The sciatic nerve consists of neuronal axons, as well as Schwann cells, fibroblasts, endothelial cells, and immune cells. Its neuronal proteome is enriched for myelination, cytoskeletal organization, and vesicle-mediated transport (STable 5). In the "myelination" terms, we see the presence of nodal and paranodal proteins such as Cntn1 (Contactin-1) and Cntnap1 (Caspr1), as well as more generally expressed neuronal proteins like Ncam1, Nefl, Nefm, and Nefh. We also see proteins more classically associated with myelin itself, such as Plp1, MBP, and MPZ , which also show expression in neuronal subtypes.[18]

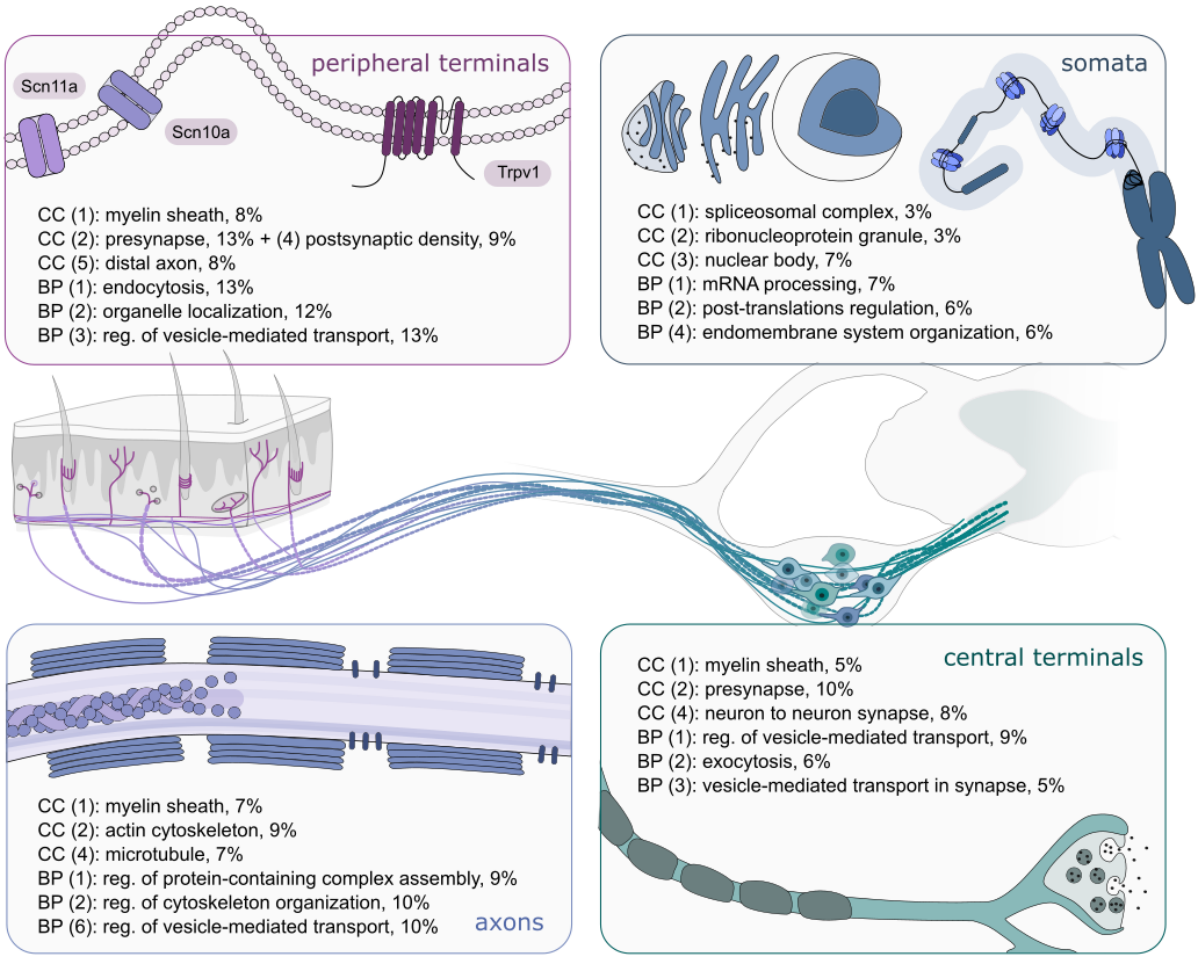

Figure 3. Pathway and neuronal subpopulation enrichment across compartments. Schematic highlights the GO over-enrichment analysis per tissue. BP = biological pathway; CC = cellular compartment. (X) term rank by adjusted p-value. % represents the GO term/neuronal enrichment. Please see STable 5 for corresponding data.

To explore functional organization across neuronal compartments, a signed weighted protein co-expression network was constructed on the neuronal proteome (Fig 4). The co-expression network was built using the WGCNA package in R with a soft power threshold of 14 (see, methods). Ten protein co-expression modules were identified (excluding the unassigned "grey" module), each comprising a minimum of 30 proteins (Fig 4A). Of these, 9 modules showed significant correlation with anatomical compartment (FDR < 0.05), while none were associated with sex (Fig 4B).

Within compartments we report significant pathway changes between males and females, as well as a few DEPs (SFig 3). The lack of sex association here suggests this is a relatively weak effect (Fig 4B), consistent with the published findings reporting a mild but present sexual dimorphism in DRG neurons.[13,19]

Specific modules showed clear compartmental specificity. For example, the brown module correlated strongly with the DRG (somata), while the blue module was

associated with central terminals in the spinal cord. Conversely, several modules - including black, yellow, and green - were negatively associated with peripheral terminals, likely indicating a relative depletion of these proteins in distal axonal endings (Fig 4C–D). As expected, most modules exhibited strong alignment with one or more anatomical compartments, reinforcing the functional specialization of the sensory neuron proteome across space (Fig 4D).

Biological pathway analyses of these modules (against a background of all proteins used to build the co-expression network) was then performed (Fig 4E-H, STable 6). The `brown` module, which is positively correlated with the soma, reflects a group of proteins implicated in `translation`, `peptide metabolic process`, and `RNA processing`(Fig 4E). The blue module, which correlated with central terminals in the spinal cord, showed associated with `trans-synaptic signalling`, `regulation of neurotransmitter levels`, and `neurotransmitter transport`, reflecting synaptic functions in the dorsal horn (Fig 4F). The yellow module, which was positively correlated with soma and central terminals, relates to `protein polymerization`, `supramolecular fibre organization` and the `regulation of cellular component size`(Fig 4G).

No modules were positively correlated with the peripheral terminals - possibly due to the lower number of enriched proteins in peripheral terminals - but the most negative correlation is the black module. Although no biological pathways reached statistical significance in this module, cellular components related to `neuronal projection`, `somatodendritic compartment`, `postsynaptic density`, and `neuronal cell body` were among the significantly enriched annotations (Fig 4H).

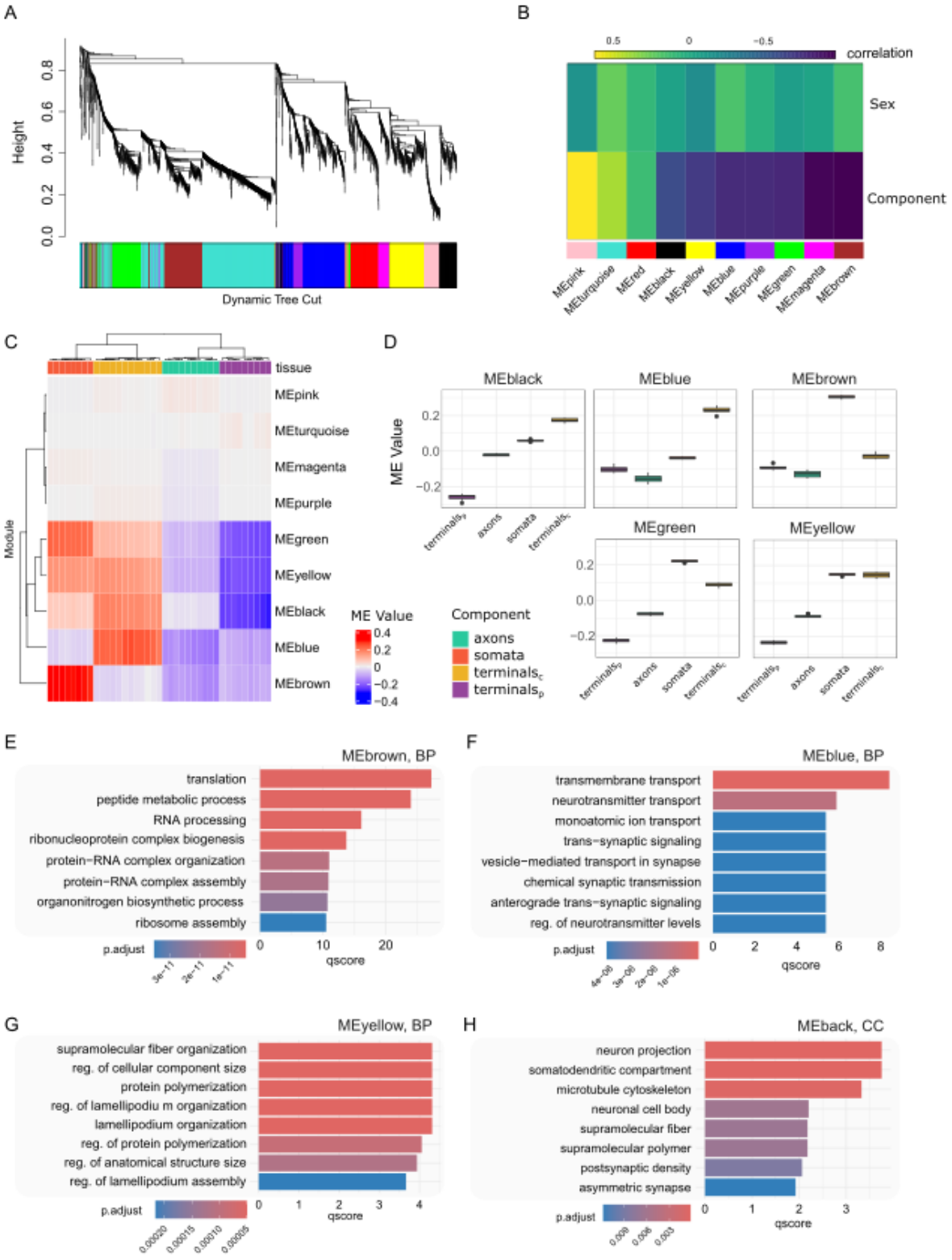

Figure 4. Weighted co-expression network of the neuronal-enriched proteome. A. Dendrogram with minimum 30 proteins per module. B. Correlation between modules and traits (compartment or sex). C. ME (module eigengene) value per sample. D. Module eigengene (ME) separation by component and module for modules significantly correlated to tissue (FDR < 0.05, BH correction). E-H. Biological pathway (E-G) and cellular compartment (H) analysis for modules of interest. E. brown, F. blue, G. yellow, H. black. No biological pathways or cellular

280 components were significant for the green module. p.adjust = adjusted p-value. qscore = -
281 log_{10}(p-value). $terminals_p$ = peripheral terminals (skin); $terminals_c$ = central terminals (SC).

282

283 *TurboID proteomics provides a unique look at terminal endings*

284 Previous -omic analyses of the skin and spinal cord have been unable to resolve the
285 molecular composition of peripheral and central terminals from primary afferents. We
286 therefore leveraged the cell type and spatial precision of the TurboID approach to
287 functionally characterize these neuronal compartments (Fig 5, SFig 4). To explore
288 protein interaction and functional organization, large-scale protein–protein interaction
289 (PPI) networks were constructed using STRING.[20] A Girvan-Newman fast greedy
290 algorithm was then used to generate community clusters[21,22], and the functional
291 enrichment of each cluster was calculated.

292 In the peripheral terminals (skin), the proteome revealed a diverse and functionally rich
293 landscape, spanning protein transport, metabolic pathways, and signal transduction
294 (Fig 5). A wide array of protein classes was detected, including SNARE complex
295 components such as Syntaxin-7 and Snap25, as well as chaperones and ubiquitin-
296 related proteins, such as Usp7 and heat shock proteins. Notably, even pain-associated
297 ion channels (Trpv1, Scn10a, and Scn11a) were detected in clusters annotated for
298 membrane trafficking and exocytosis. A full breakdown of each cluster enrichment is
299 available in STable 7.

300 A similar pattern was observed in the central terminals (spinal cord; LSC), where
301 clustering revealed extensive functional heterogeneity (SFig 4, STable 8). Enriched
302 clusters included pathways involved in signal transduction, endosomal processing, and
303 membrane trafficking—hallmark processes of synaptic signalling and
304 neurotransmission (see Stable 8 for a functional breakdown). Together, these analyses
305 demonstrate that proximity labelling via TurboID enables unprecedented access to the
306 proteomic architecture of otherwise inaccessible neuronal compartments. This
307 approach holds considerable promise for extracting functional, spatially resolved
308 proteomes in defined cell types.

309 *TurboID proteomics distinguishes neuronal proteomes from bulk tissue backgrounds*

310 To contextualize the advantages of TurboID-based proximity labelling, we compared our
311 compartment-resolved neuronal proteomes to conventional bulk tissue proteomics.
312 We harvested the skin, SCN, DRG and SC and determined the proteome using the same
313 mass spectrometry-based workflow as applied to the TurboID samples above (SFig 5,
314 STable 9). As expected[23,24], we detect several thousands (7000-9000) protein groups per
315 tissue (SFig 5A), with samples clustering by tissue (SFig 5B). Consistent with earlier
316 studies[23,24], we identified many neuronal proteins in bulk datasets. Overall, these bulk
317 tissue proteomes exhibited a large overlap with neuronal proteomes defined by our

318 TurboID approach (Fig. 1-4), while dozens of proteins were identified uniquely in each
319 neuronal proteomes (SFig 5D, STable 10).

320 *TurboID proteomics depletes non-targetted cell type proteomes*

321 The TurboID workflow enables us to selectively define the neuronal proteome within
322 heterogeneous tissue (Fig 2-5, STable 10). To confirm the enrichment of sensory
323 neurons under the Advillin driver, we also investigated the depletion of immune
324 subtypes across compartments (SFig 6). ImmuCellAI[25] was used to calculate an
325 "immune infiltration score", which reflects a composite GSEA enrichment across
326 immune subtypes. In every compartment, we see a reduced immune signature
327 (compared to bulk tissue samples), further validating our approach (SFig 6).

328 This highlights two key advantages of TurboID-based neuronal enrichment: First, it
329 facilitates the discrimination of proteins expressed in neurons versus non-neuronal
330 cells within the same tissue. Second, TurboID enhanced detection sensitivity in tissues
331 with sparse neuronal content, such as in the skin. In these regions, the detection of
332 sensory neuron-specific proteins — particularly ion channels — has been challenging
333 and largely unsuccessful using bulk proteomics.[23,26] In contrast, TurboID-based profiling
334 recovered functionally important signatures in peripheral terminals, including
335 prominent drug targets such as Scn10a, Scn11a, and Trpv1, providing molecular access
336 to previously inaccessible compartments (Fig 5, SFig 5D).

337 Together, these data underscore the power of TurboID-based proteomics to resolve cell
338 type-specific proteomes within complex tissues, particularly for rare or spatially
339 restricted compartments. Importantly, this strategy opens a path to study the proteome
340 dynamics of afferent terminals in disease models and in response to pharmacological
341 interventions. Beyond sensory neurons, our TurboID$^{fl/fl}$ workflow can be readily adapted
342 with other driver lines to define functionally relevant, compartment-specific proteomes
343 across diverse tissues and cell types.

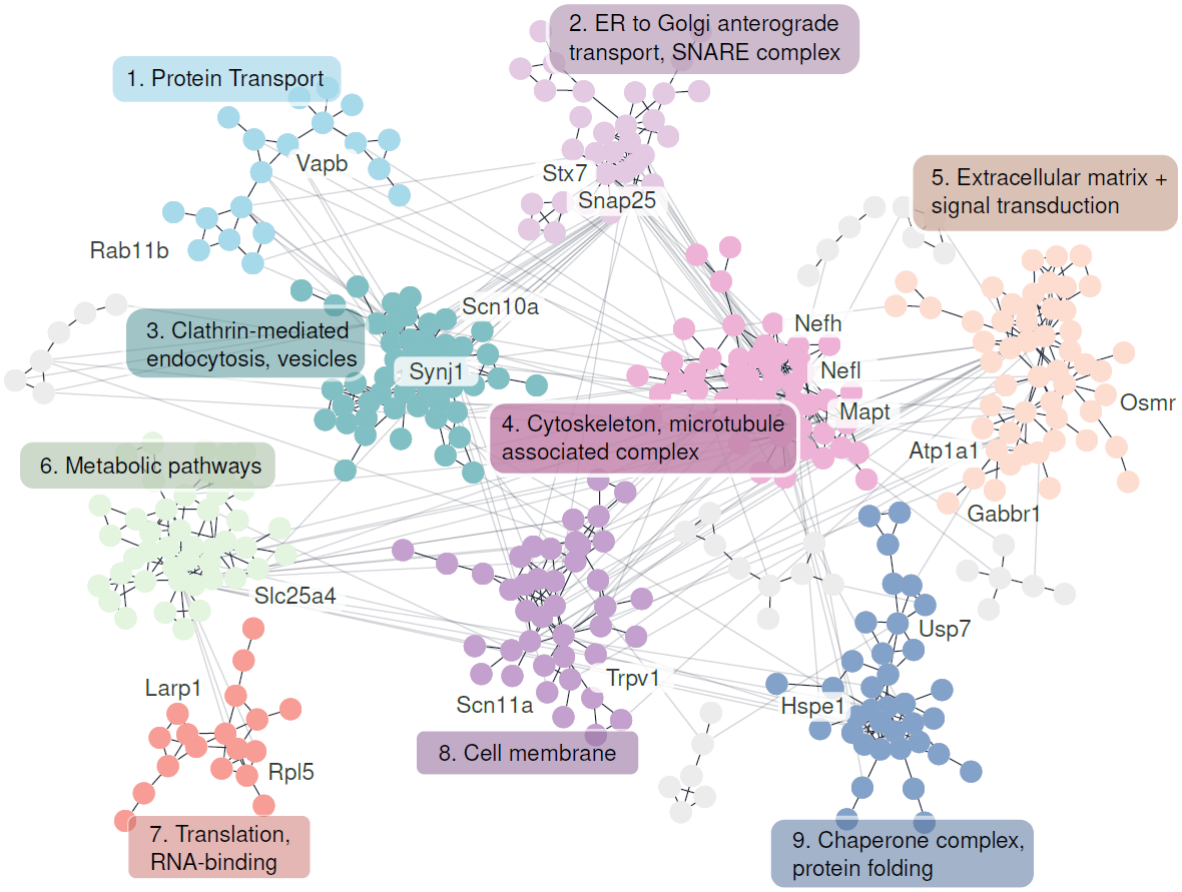

Figure 5. Community clustering of the peripheral terminal proteome, with edges denoting high confidence protein-protein interactions. Protein nodes are coloured by cluster, and clusters are described by functional summaries with proteins of interest highlighted. Full functional enrichments are available in STable 7.

TurboID proteomics reveals neuronal-specific changes in response to oxaliplatin treatment

Next, we aimed at showcasing the utility of our TurboID workflow to assess neuronal proteome changes in a pharmacological context. For this, we turned to oxaliplatin, a chemotherapeutic agent. Chemotherapy-induced peripheral neuropathy (CIPN) is a common and often painful condition affecting the peripheral nervous system, known to impact neuronal and non-neuronal cells in the DRG.[12] In adherence to the 3Rs of animal research, we employed a DRG explant model to explore oxaliplatin-induced changes in the neuronal somata (Fig 6, SFig 7-8, STables 11-16).

Mirroring the compartmental proteomes above, we determined the bulk proteome of DRG explants from wildtype mice and compared these data with neuronal proteomes obtained from Adv^{Cre};TurboID$^{fl/fl}$ mice. In the bulk proteome of wildtype mice we identified ~7200 protein groups (SFig 7A, STable 11), with clustering driven by oxaliplatin concentration (SFig 7B-C). Consistent with earlier studies, oxaliplatin exposure led to

widespread proteome changes, including alterations in known neuronal proteins (SFig 7D-E, STable 12). When comparing differentially expressed proteins (DEPs) from our DRG explant data to previous work *in vivo*[27], we see a strong correlation between the general expression of these proteins (SFig 7F). We next employed a rank-rank hypergeometric overlap test to compare the differential protein expression from their *in vivo* data to ours (SFig 7G). This shows good concordance for protein changes across both datasets, suggesting similar regulation by oxaliplatin and validating our *in vitro* approach.

In DRG explants from Adv^{Cre};$TurboID^{fl/fl}$ mice, we observed specific alterations of the neuronal explant proteome in response to oxaliplatin (Fig 6, SFig 8, STable 13). As expected, Adv^{Cre};$TurboID^{fl/fl}$ explants exhibited prominent protein enrichment compared to $TurboID^{fl/fl}$ controls (SFig 8A). Samples clustered by genetics in the first principal component (PC), with slight separation by drug treatment in the second PC (SFig 8B). In both oxaliplatin-treated (SFig 8C, left) and vehicle-treated (SFig 8C, right) explants, Adv^{Cre};$TurboID^{fl/fl}$ samples (vs $TurboID^{fl/fl}$) showed robust enrichment of neuronal proteins with ~ 2500 protein groups per condition (SFig 8D, STable 14).

Within the neuronal explant proteome, we detected a substantial number of DEPs after oxaliplatin treatment (Fig 6A, STable 15). Notably, these differences were only partially reflected in the bulk explant proteome (Fig 6B). Even so, we saw a high rank-rank hypergeometric overlap between the bulk explant and neuronal proteomes after oxaliplatin treatment (Fig 6C), and a high semantic similarity across DEPs (Fig 6D).

Next, we assessed DEP-associated functions. After oxaliplatin treatment, pathways related to amino acid transport and cell adhesion were downregulated in the neuronal explant proteome (Fig 6E, STable 16). To further dissect these pathways, we constructed a corresponding PPI network based on pathway-associated DEPs (Fig 6F). This revealed prominent downregulation across multiple functional modules (Fig 6Fi). While some of these DEPs were detected in both bulk and neuronal explant proteomes, others were uniquely regulated in the neuronal proteome (Fig 6Fii). The latter includes Trpv1, Scn11a, and Calca, as well as the central module with Itgb1, Tin2, and Rock2. These findings illustrate the enhanced resolution of cell type-specific proteomics using TurboID, uncovering molecular changes that may be masked in bulk tissue analyses.

In summary, targeted cellular proteomics can uncover relevant proteomic differences across compartments and pharmacological treatments, offering a powerful tool to dissect disease mechanisms and treatment effects in complex tissues.

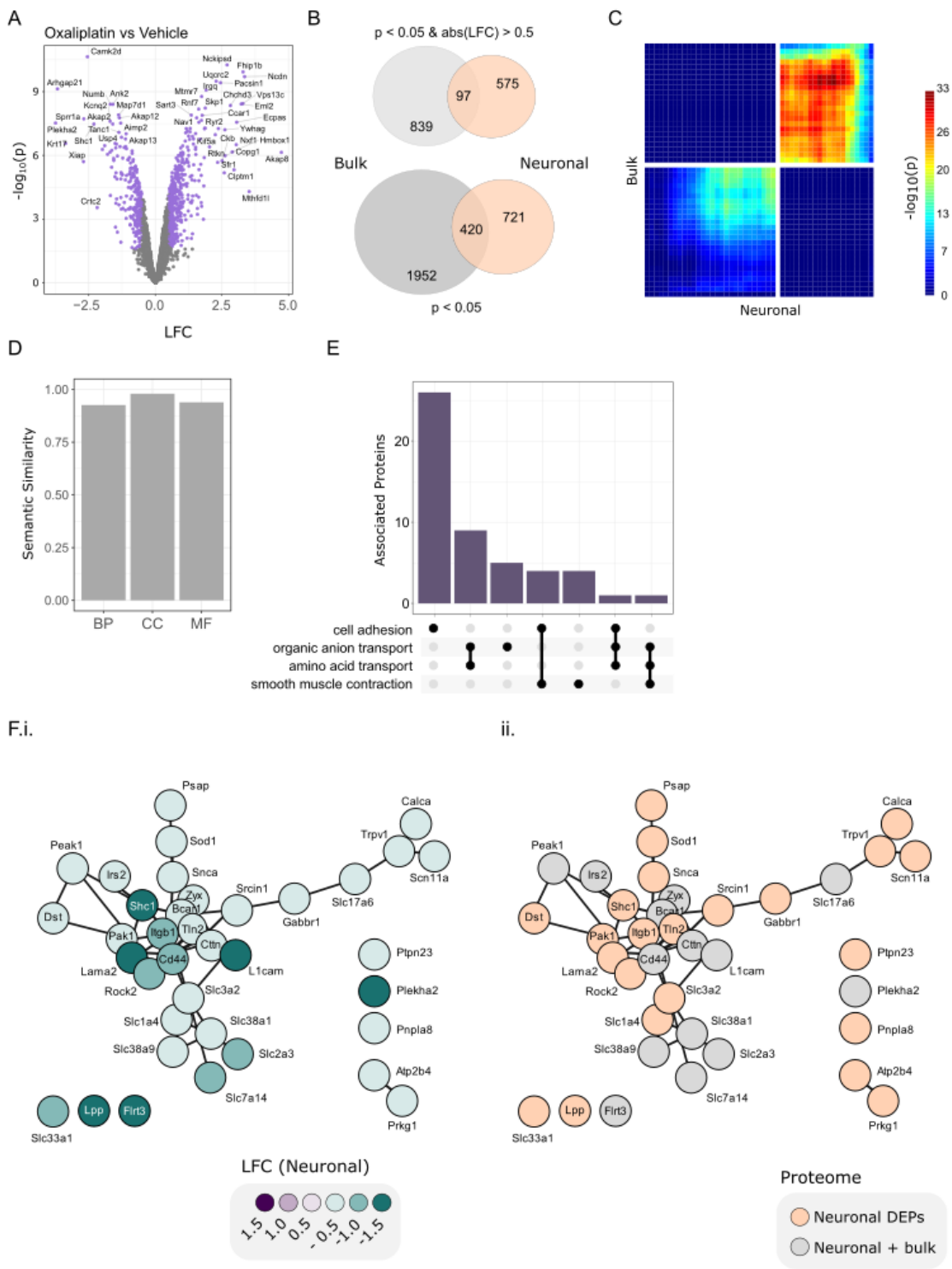

Figure 6. Oxaliplatin-treated Adv^{Cre};TurboID$^{fl/fl}$ explants highlight neuronal dysregulation. A. Volcano plot for oxaliplatin vs vehicle, neuronal proteome (Adv^{Cre};TurboID$^{fl/fl}$). B. DEP overlap (oxaliplatin vs vehicle) between bulk (WT, grey) and neuronal (Adv^{Cre};TurboID$^{fl/fl}$, orange) explant proteomes. C. Correlation between LFC for overlapping DEPs in B. D. Semantic similarity between neuronal and bulk DEPs. E. Neuronal biological pathway downregulation after oxaliplatin treatment, highlighting protein counts which overlap across pathways. F. STRING protein-protein interaction network for DEPs in regulated pathways from E. i, LFC from neuronal

proteome. ii, Specificity to neuronal analysis. DEPs detected only in Adv^{Cre};TurboID$^{fl/fl}$ are in orange, those overlapping with the bulk analysis are grey.

Discussion

As a generalized proof-of-concept, we demonstrate how a TurboID transgenic mouse enables cell-type-specific proteomic labelling across anatomically distinct compartments. When paired with Advillin^{Cre}, TurboID expression is targeted to primary sensory neurons of DRG, resulting in robust, neuron-enriched biotinylation. Using DIA-PASEF mass spectrometry, we profiled compartment-specific DRG proteomes and uncovered enrichment of neuron-specific proteins and pathways. These included canonical markers and functionally relevant processes, such as translation in the somata and neuron-to-neuron synapse functions in the central terminals of the spinal cord.

This spatial resolution is particularly significant in the peripheral terminals of DRG neurons in the skin. These nerve endings are typically characterized by immunohistochemistry and have remained largely inaccessible to unbiased omics approaches. Neither our bulk proteomic data nor previous high-coverage DIA-MS datasets from mouse skin[23] or human skin[26] detected key sensory neuron markers. In bulk analyses, low-abundance neuronal signatures are often masked by dominant cell types. Using TurboID-based proteomics, we were able to detect key markers and drug targets such as Trpv1, Scn10a, and Scn11a in the peripheral terminals.

While single-cell and single-nucleus RNA sequencing are valuable for cell-type-resolved transcriptomes[28,29], they are limited to somata within the DRG, lack proteomic resolution, and do not capture distal compartments. [28,29] The expansion of spatial sequencing helps address many of these issues, although recent spatial transcriptomics of the sciatic nerve have not resolved neuron-specific clusters[30], and to our knowledge, a high resolution spatial-seq dataset including peripheral terminals in the skin is still missing. As these methods mature, they will complement our data well. At present, however, our TurboID-based proteomic atlas offers a unique spatial profile spanning the full extent of mouse sensory neurons. While not a main focus of this study, we were also able to probe neuronal sex differences across compartments, expanding on previously reported sexual dimorphism in mouse and humans.[13,19,23,31] Mirroring recent transcriptomic data across sensory neuron subtypes, we see some, but not extensive differences between male and female neurons.[13] Few proteins were sexually dimorphic within compartments, including Kct2 in the soma and Brd4 in the peripheral terminals (both enriched in females), as well as Serpina3k in the axon (enriched in males). Previous bulk proteomic analyses of mouse sciatic nerve and paw have also identified Serpina3k enrichment in males[23], although no DEPs from the paw were shared with their bulk data, suggesting a unique signature from the peripheral terminals versus whole skin preparations.[23] In the central terminals of the spinal cord, we see an

449 enrichment of Lgi1 and Sprr1a in males. Sprr1a is an injury marker with reported male-
450 biased mRNA expression in DRG[13], though the functional consequences remain to be
451 defined. Lgi1 has recently been implicated in pain sensitivity[25], and future studies are
452 needed to investigate whether the proteomic differences observed here translate to
453 phenotypic effects.

454 To highlight how this resource could be exploited to study functional changes in a
455 clinically-relevant disease context, we next studied neuronal changes in a DRG explant
456 model of CIPN. Exposure to oxaliplatin resulted in widespread proteomic alterations in
457 both bulk and neuron-enriched samples. While the sets of differentially expressed
458 proteins (DEPs) varied between bulk and TurboID-labelled samples, semantic similarity
459 of enriched pathways was high, indicating shared biological responses. A major benefit
460 of the Adv^{Cre};$TurboID^{fl/fl}$ approach in explants is the cell type specificity, highlighting
461 disruption to organic anion and amino acid transport pathways in neurons. This
462 contrasts the more generalized effect of oxaliplatin seen in the whole DRG proteome,
463 where we lose the cell type resolution.

464 Transporter disruptions have widely been reported in the context of CIPN.[12,32–36] Organic
465 cation transporters, such as Oct2, have been implicated in oxaliplatin uptake by
466 sensory neurons, and their activity contributes to neurotoxicity.[12,36] Similarly, organic
467 anion-transporting polypeptides (OATPs) affect CIPN pathophysiology.[32,37,38] Impaired
468 transporter function can lead to drug accumulation in DRG, contributing to
469 mitochondrial dysfunction, oxidative stress, and neuroinflammation, all of which
470 underlie CIPN pathogenesis.[12] In our study, several transporters were downregulated in
471 response to oxaliplatin treatment. Some changes are evident across neuronal and bulk
472 proteomes (e.g. Slc7a14, Slc2a3), while the dysregulation of others (e.g. Slc1a4, Slc3a2,
473 Slc33a1) could only be detected when studying the neuronal proteome. Pursuing these
474 transport pathways may provide novel strategies to mitigate CIPN while preserving the
475 anticancer efficacy of chemotherapy, with promising attempts to target transporters
476 already in development.[37]

477 Finally, our findings highlight the practicality of the DRG explant model for rapid *in vitro*
478 screening of neurotoxic effects. It also reinforces the added value of compartment-
479 specific proteomics in detecting functionally relevant molecular changes. When paired
480 with conventional bulk analyses, our approach offers a multi-layered view of the
481 proteomic landscape in response to drug treatment and in disease models,
482 complementing and extending previous *in vivo* work.[27]

483

484 *Limitations*

485 This study provides a quantitative, compartmental proteomic atlas of DRG sensory
486 neurons and serves as a valuable reference for the field. However, it is likely not
487 exhaustive. Detection of low-abundance proteins may be further improved through

488 advances in mass spectrometry sensitivity, biotinylation efficiency, and sample
489 preparation protocols. As expected, fewer protein identifications were obtained in
490 peripheral terminals and axons - a likely reflection of tissue composition and neuronal
491 content - resulting in a relative bias toward somata and central terminals, where
492 neuronal protein density is higher. While these results represent a robust starting point,
493 future studies with deeper coverage and within-compartment comparisons under
494 various biological conditions will be critical for advancing our knowledge about the
495 molecular features of terminal regions.

496 *Future directions*

497 A key advantage of using TurboID transgenic mice is the opportunity to interrogate
498 otherwise inaccessible cellular compartments. Prior work in both mice and humans has
499 shown alterations in intraepidermal nerve fibre density across painful conditions.[1,39]
500 Pairing our compartmental proteome with *in vivo* functional testing (e.g. oxaliplatin
501 administration) will provide a rich understanding of the underlying molecular changes
502 and their correlation with behavioural outcomes in future studies.

503 Another major benefit lies in the fact that Cre-based recombination allows flexible
504 customisation. Pseudobulk analyses are frequently used in scRNA-seq (and spatial)
505 transcriptomics to compare within cell-type changes across conditions. Paired to
506 adequate transgenic drivers and downstream DIA-MS, TurboID$^{fl/fl}$ can be used to
507 generate a corresponding proteome for multi-omic analyses within cell types. In the
508 context of sensory neurons, this can be subtype targeting (e.g. Mrgprd^{Cre} or Th^{Cre}) or
509 injury-specific targeting (e.g. Atf3^{Cre}).[14,40] More broadly, our approach could be extended
510 to diverse cell types, such as fibroblasts in the skin, satellite glia in the DRG, or
511 interneurons in the dorsal horn (to name a few).

512 **Conclusions**

513 In this study, we generated a TurboID$^{fl/fl}$ transgenic mouse, using it to systematically
514 profile the proteomes of DRG sensory neuron compartments. Spanning from peripheral
515 to central terminals, this study presents a proteomic atlas across DRG sensory neuron
516 compartments. Our findings reveal compartment-specific protein distributions that
517 reflect specialized neuronal functions. Furthermore, we report previously unknown
518 neuron-specific changes in an explant model of chemotherapy-induced peripheral
519 neuropathy. Taken together, our methodological workflow and obtained data serve as a
520 highly valuable resource for studying neuronal specialization and proteome dynamics in
521 the peripheral nervous system.

522 **Code Availability**

523 All code is available at https://github.com/aliibarry/turboID.

524 **Data Availability**

525 The mass spectrometry proteomics data, including metadata, fasta, and gene group
526 matrices for each dataset have been deposited to the ProteomeXchange Consortium
527 via the PRIDE[41] partner repository with the dataset identifier PXD062198. Processed
528 data are also available on github (https://github.com/aliibarry/turboID/data/).

529 For queries regarding the TurboID mice please contact Nils Brose
530 (brose@MPINAT.mpg.de) or Noa Lipstein (lipstein@FMP-berlin.de).

531 **Acknowledgements**

532 The authors would like to thank Christiane Harenberg, Dayana Warnecke and Mia
533 Wzietek from the AGCTLab (Department of Molecular Neurobiology, Max Planck
534 Institute, MPI, for Multidisciplinary Sciences, Goettingen) for expert technical
535 assistance and genotyping, as well as Nicole Kanta and Sabrina Grundtner (University
536 of Vienna) for their excellent assistance. We are grateful to the staff of the animal house
537 of the MPI and of the mouse house at the Division of Pharmacy (University of Vienna) for
538 expert mouse husbandry and support. We further thank Dr. Kimmina, Dr. Schraepler,
539 Dr. Fuenfschilling and Dr. Papadopoulos (all at MPI) for their support in all mouse-
540 related issues, as well as Elham Barkhordar and Dr. Dominic Winter (University of Bonn,
541 Germany) for initial discussions about the BioID approach. We thank all members of the
542 Schmidt laboratory for fruitful discussions.

543 This work was funded in part by the Austrian Science Fund (FWF) [10.55776/P36554] (to
544 MS), the University of Vienna (to MS), the Max Planck Society, the German Research
545 Foundation, Excellence Strategy EXC-2049–390688087 (to NL), and CRC 1286
546 "Quantitative Synaptology", project A11 (to NL) and A09 (to NB).

547 **Author Contributions**

548 Method optimization, sample preparation and data collection were performed by JRS
549 with input from FX, DVG, and MS. Analyses were performed by AMB, with input from JRS,
550 FX, and MS. Mass spectrometry was performed by FX with input from JRS and DGV.
551 Conceptualization and funding acquisition by MS with input from DGV. Oxaliplatin
552 experiments were performed by JRS and TH. TurboID$^{fl/fl}$ mice were conceived, designed,
553 generated and validated by NB, FB, DS, and NL. Manuscript was written by AMB, JRS,
554 and MS. All authors approved the submitted version.

555 **Declaration of interests**

556 The authors declare no conflicts of interest related to this work. NL is a scientific
557 advisory board member of TRACE Neuroscience inc. MS and DGV maintain an ongoing
558 scientific collaboration with Bruker, but this collaboration had no influence on the
559 content of the manuscript.

560

561

562

563 **Methodology**

564 *Generation of TurboID mice (ROSA26$^{em1(TurboID)Bros}$) using CRISPR/Cas9*

565 The conditional TurboID knock-in (cKI) mouse line was generated by site-directed
566 CRISPR/Cas9 mutagenesis in the ROSA26 locus. Superovulated FVB/J females were
567 mated with FVB/J males and fertilized eggs collected. In-house produced CRISPR
568 reagents (hCas9_mRNA, sgRNAs, preformed Cas9_sgRNA-RNP complexes and the
569 homology-directed repair fragment (HDR fragment)) were microinjected into the
570 pronucleus and the cytoplasm of pronuclear-stage zygotes using an Eppendorf
571 Femtojet. Importantly, all nucleotide-based CRISPR/Cas9 reagents (sgRNAs and
572 hCAS9_mRNA) were used as RNA molecules and were not plasmid-encoded, reducing
573 the probability of off-target effects due to the short lifetime of RNA-based reagents.[42,43]
574 The TurboID-containing HDR fragment was generated by subcloning a V5-tag-TurboID
575 sequence into the Ai14-ROSA26-based plasmid backbone[44] and isolated as a linear
576 DNA fragment by SacI/AgeI restriction enzyme double digestion. Two sgRNAs targeting
577 the ROSA26 Locus were selected using the guide RNA selection tool CRISPOR.[45,46] The
578 correct locus-specific insertion of the HDR fragment was confirmed by localization
579 PCRs with primers upstream and downstream of the HDR sequence. Extended details,
580 including full sequences and genotyping strategy, are available in the Supplemental
581 Methods.

582 *Animal husbandry*

583 Adult male and female TurboID$^{fl/fl}$ control/ Adv^{Cre};TurboID$^{fl/fl}$ mice (12.5-26 weeks old for
584 compartmental proteome, 57-71 weeks old for oxaliplatin part) and in-house bred wild
585 type C57BL/6J male mice (60-66 weeks old) were kept in a 12/12h day/night cycle with
586 *ad libitum* access to food and water in an open-cage environment. TurboID$^{fl/fl}$ control
587 and Adv^{Cre};TurboID$^{fl/fl}$ mice received biotin-enriched drinking water (0.22 mg/mL,
588 prepared freshly every day) for 7 consecutive days and on day 8 the mice were
589 sacrificed.

590 The animal experiments were conducted in accordance with ethical guidelines and
591 were approved by the Institutional Animal Care and Use Committee (IACUC) at the
592 University of Vienna and the Austrian Ministry for Education, Science, and Research
593 (BMBWF; license number 2021-0.138.925 amended by 2024-0.896.105). All procedures
594 complied with the international ARRIVE guidelines and adhered to the European Union
595 Directive 2010/63/EU on the protection of animals used for scientific purposes. No mice
596 were removed from the study before their expected endpoint.

597 The compartmental proteome was generated from pooled samples (4-6 per samples
598 per group per tissue) from the following mice: TurboID$^{fl/fl}$ control = 29M + 29F and
599 Adv^{Cre};TurboID$^{fl/fl}$ = 19M + 27F.

600 Unilateral mouse DRG were used for one explant culture stimulated with Oxaliplatin,
601 the DRG of the other side for the Vehicle condition in parallel. For the enrichment of
602 biotinylated proteins in Adv^{Cre};$TurboID^{fl/fl}$, 4 samples (3M, 1F) were prepared for each
603 condition, with multiple mice pooled for each samples. In total, 10 males and 4 females
604 were used per condition (3-4 mice per sample).

605 *Tissue dissection*

606 Mice were sacrificed via CO_2-inhalation and rapidly decapitated. The vertebral spine
607 was removed for subsequent isolation of the dorsal part of the lumbar 3-5 spinal cord
608 (SC) and lumbar 3-5 dorsal root ganglia (DRG). In parallel the sciatic nerves (SCN) of
609 both sides were dissected. The plantar paw skin (dermis and epidermis, without muscle
610 tissue) was removed by a 4 mm skin punch. Skin samples were immediately snap-
611 frozen in liquid N_2, all other tissues were washed in ice-cold 1× PBS to remove blood
612 residuals before snap-freezing in liquid N_2. All tissues remained at -80°C until further
613 use.

614 *Protein extraction*

615 All steps are done at room temperature (RT) except otherwise mentioned.

616 DRG: Tissue homogenisation was done in lysis buffer (LB; 2% SDS, 0.1 M tris, 5%
617 glycerol, 0.01M DTT, 1× complete protease inhibitor cocktail) with 3x 10 strokes of a
618 pestle/potter. To facilitate lysis the homogenate was sonicated using a Bioruptor Pico
619 (10x 30 s ON/30 s OFF, 4°C, low frequency, all sonification steps mentioned below are
620 done with the same settings, only cycle number varies) and further incubated at 70°C,
621 for 15' min with 1500 rpm (this and all other incubation with agitation were done in a
622 Thermomixer C, Eppendorf). The remaining cell debris was pelleted by centrifugation
623 (10', 10000 ×g) and the supernatant was saved. All replicates of one condition were
624 pooled and the concentration determined at 280 nm with a NanoPhotometer N60
625 (Implen, München, Deutschland).

626 SCN: Protocol was performed as above, except the centrifugation was followed by
627 another 5moin-long centrifugation (RT, 10000×g) to further clear the lysate of lipid
628 clouds. Before pooling and concentration measurement an acetone precipitation was
629 done (see below).

630 SC: The DRG protocol was modified in that the pestle/potter step was omitted, instead
631 the SC was cut into 3 smaller pieces and transferred to 2 mL LoBind tubes (prefilled with
632 500 µL of LB) for sonification Pico for 15 cycles. Other steps as for DRG, but before
633 pooling and concentration measurement an acetone precipitation was done (see
634 below).

635 Paw skin: the skin punches were cut into 4 smaller pieces, transferred into a potter
636 prefilled with LB and homogenized with help of 3× 10 strokes of a pestle/potter. Lysis of
637 tissue was facilitated by incubation for 20 min, at 70°C and 1500 rpm, followed by

638 sonification for 15 cycles. The lysate was cleared off cell debris and excessive lipids by
639 2× centrifugation 10 min, 10000×g) and the supernatant was saved. Before pooling and
640 concentration measurement an acetone precipitation was done (see below).

641 For the SCN, SC and paw skin an acetone precipitation was done to reduce the amount
642 of lipids in the samples: 5× sample volume of pre-cooled (-20°C) 100% acetone was
643 added to each sample and the tube was shortly inverted to ensure thorough mixing. If
644 needed, samples were split into 2× 2 mL tubes to allow for 5× addition of sample
645 volume. Precipitation of proteins was allowed for 3-3.5 h at -20°C. Next the precipitates
646 were pelleted by centrifugation for 30 min and 14000×g. Pellets were washed with 1.5
647 mL pre-chilled (4°C) 80% ethanol and the centrifugation repeated as above. After
648 removal of the ethanol, pellets were air-dried for 20-30 min. Proteins were reconstituted
649 in LB by incubation for 15 min, 70°C, 1500 rpm. If were not fully solubilized, the
650 incubation was repeated and LB volume increased until fully solubilized. Total protein
651 concentration of pooled samples was determined with a NanoPhotometer at 280 nm.

652 *Streptavidin-mediated enrichment of biotinylated proteins*

653 Streptavidin-affinity purification protocol is based on the high stringency protocol
654 described in Go et al., 2021 with modifications. The required amount of streptavidin
655 beads (Sera-Mag SpeedBead Blocked Streptavidin Particles, Cytiva, 83 µL bead slurry/
656 1000 µg input) was transferred into LoBind protein tubes, washed twice with 500 µL LB
657 without SDS, and resuspended in the same buffer. Protein lysates (input amount: DRG
658 1000 µg, SCN 600 µg, SC 800 µg, skin 2000 µg) were prepared in a way that the final SDS
659 concentration was 0.5% in a final volume of 1500 µL and incubated with the beads at
660 4°C for 3.5 h on an overhead shaker. Unless otherwise stated, all subsequent steps
661 were performed at RT.

662 Following incubation, samples were placed on a magnetic rack for 2 min. Beads were
663 then subjected to a series of washes, each performed with 1 mL of buffer, followed by
664 overhead shaking for 1 min each (Grant-Bio PTR-35 Multi-Rotator)and incubation on the
665 magnetic rack for 2 min until the solution cleared. The washes included one step with
666 2% SDS Wash Buffer (2% SDS, 25 mM Tris), two washes (three for skin samples) with
667 modified RIPA buffer (50 mM Tris, 150 mM NaCl, 1.5 mM $MgCl_2$, 1% Triton X-100, 1 mM
668 EDTA), and three washes with 50 mM ammonium bicarbonate (ABC, pH 8). After the first
669 ABC wash, the beads were transferred to a new 1.5 mL LoBind tube in 500 µL ABC
670 buffer, followed by the addition of another 500 µL ABC before finalizing the washes.

671 For protein reduction, 135 µL of 5 mM dithiothreitol (DTT) in 50 mM ABC containing 0.8
672 mM biotin was added to each sample and incubated at 60°C for 30 min at 1000 rpm.
673 Samples were then cooled to RT by briefly placing them on ice. Alkylation was
674 performed by adding iodoacetamide (IAA) to a final concentration of 20 mM (15 µL of
675 200 mM IAA), followed by incubation for 30 min in the dark under constant agitation. The
676 reaction was quenched by adding 1M DTT to a final concentration of 5 mM and

677 incubating for 15 min with 3× 5 s vortexing steps in between. Proteins were digested for
678 17 h at 37°C and 950 rpm using 1.5 µg Trypsin/LysC per 1000 µg input. After the digest,
679 peptides were eluted by placing the tubes on a magnetic rack for 2 min and transferring
680 the supernatant to fresh 2 mL LoBind tubes. The beads were further washed with 20 µL
681 MS-grade water (5 min, 500 rpm), and the wash was pooled with the initial eluate.
682 Peptide concentrations were measured at 205 nm to calculate the required amount of
683 SP3-beads (1:1 mix of Sera-Mag SpeedBead beads, 10-15 µL bead slurry to 40-50 µg
684 peptides). To clean-up the peptides, peptide solution was split into two 2 mL tubes, the
685 required bead amount and 100% ACN was added to reach 95% ACN. Samples were
686 incubated for 8 min and 500 rpm, followed by a 2-min incubation on a magnetic rack.
687 The ACN was discarded, and beads were rinsed with 400 µL 100% ACN, incubated for 2
688 min on a magnetic rack, and the ACN was discarded again. Peptides were reconstituted
689 in 20-25 µL MS-grade water, incubated for 5 min with shaking at 500 rpm, followed by
690 another 2-min incubation on a magnetic rack. The supernatants of previously split
691 samples were pooled, centrifuged at 17000×g for 2 min, placed on a magnetic rack, and
692 the final supernatant was transferred to a glass vial. Peptide concentrations were
693 measured at 205 nm with a NanoPhotometer, and samples were acidified to a final
694 concentration of 0.1% formic acid (FA). The samples were stored at -20°C until LC-MS
695 measurement.

696 *DRG explants preparation*

697 From both Adv^{Cre};TurboID$^{fl/fl}$ and TurboID$^{fl/fl}$ mice (fed with biotin-enriched water for 7
698 days, see above) 20 DRG per side were isolated and collected separately by side in two
699 tubes containing DMEM/F-12 at RT. The DRG of one side were plated in 50 µL volume in
700 to a well of a 24-well plate and incubated for 10 min at 37°C, 5% CO_2. In the meantime,
701 the oxaliplatin (100 µM) and/or vehicle (H_2O, Veh) was mixed with DMEM +10% horse
702 serum (HS) +100 ng/mL nerve growth factor (NGF) + 50 µM biotin and 500 µL/well were
703 carefully added. The drug/Veh was incubated for 48 h at 37°C, 5% CO_2.

704 To find an effective oxaliplatin concentration in line with previous reports[47], DRG explant
705 cultures were prepared in a similar way from wild type mice. DRG from one mouse were
706 separated into 4 wells for 4 conditions Veh, 25 µM, 50 µM and 100 µM oxaliplatin in
707 DMEM+HS+NGF. The drug/Veh was incubated for 48 h at 37°C, 5% CO_2.

708 *Sample preparation of DRG explants*

709 The protein extraction was done similarly for both WT and TurboID DRG explants. All
710 DRG of one well were transferred to an Eppendorf tube and washed twice with ice-cold
711 1× PBS by inverting the tube 10×. After discarding all PBS, 300 µL LB was added and
712 DRG explants were sonicated for 10 cycles and further incubated at 70°C, for 15 min
713 and 1500 rpm. Remaining cell debris was pelleted by centrifugation (5', 10000×g) and
714 the supernatant was saved. The total protein concentration was determined at 280nm
715 with a NanoPhotometer N60. The TurboID samples underwent the above described

716 streptavidin-affinity purification to enrich for biotinylated proteins and preparation of
717 peptides (input 725 µg).

718 For the WT samples a modified version of the single-pot, solid-phase-enhanced sample
719 preparation (SP3) method[48] was employed to digest proteins and clean the peptides. In
720 brief, 10 µL of pre-mixed Sera-Mag SpeedBead beads were added to 50 µg of protein. To
721 facilitate protein binding to the beads, an equal volume of absolute ethanol was added,
722 followed by incubation for 5 min at 24°C and 1000 rpm. Beads were collected on a
723 magnetic rack for 2 min, the supernatant was discarded, and the beads were washed
724 thrice with 500 µL of 80% ethanol. Subsequently, the beads were resuspended in 50 µL
725 of 50 mM ABC, pH 8 containing 2 µg of Trypsin/Lys-C and incubated overnight at 37°C
726 and at 950 rpm. Following protein digestion, ACN was added to each sample to reach a
727 final concentration of 95%. After an 8-min incubation, beads were collected on a
728 magnetic rack for 2 min. The supernatant was discarded, and the beads were washed
729 with 900 µL of ACN. For peptide elution, the remaining ACN was allowed to evaporate
730 for 2-3 min and the beads were resuspended in 40 µL of LC-MS grade water. Peptide
731 concentrations were measured at 205nm using a NanoPhotometer N60. Finally, the
732 peptide samples were acidified with FA to a concentration of 0.1% and stored at -20°C
733 until LC-MS/MS analysis.

734 *Gel-electrophoresis & Western blot*

735 All lysates from TurboID tissue that were going to be used as input samples for the
736 streptavidin-affinity enrichment were checked by WB for the biotinylation success. The
737 samples were prepared by dissolving them in 4× LDS Sample Buffer supplemented with
738 4× Reducing Agent to reach final 1×concentrations followed by heating to 70°C for 10
739 min. For protein separation, samples were loaded onto pre-cast NuPAGE® Bis-Tris 4–
740 12% gradient gels, the NuPAGE® (Life Technologies) electrophoresis chambers filled
741 with 1× NuPAGE® MOPS buffer and the gels run for 40-50 min at 200 V.

742 Following electrophoresis, proteins were transferred onto PVDF membranes using the
743 iBlot2® Gel Transfer Device (Life Technologies, program #0, 7 min). To block non-
744 specific binding sites, membranes were incubated with 5% milk in PBS for 45 min at RT.
745 Subsequently, membranes were incubated with primary antibodies (diluted in 1%
746 milk/PBS; Stable 1) for 1.5 h, followed by an overnight incubation at 4°C with an
747 additional 1:4 dilution. Membranes were washed with PBS (three short washes followed
748 by three 5-min washes) before incubation with the respective secondary antibodies
749 (diluted in 1% milk/PBS; see Stable 1) for 1 h. After washing with PBS as described
750 before, immunolabeled proteins were detected using near-infrared fluorescence
751 imaging (BioRAD ChemiDoc MP).

752 *LC MS acquisition*

753 Nanoflow reversed-phase liquid chromatography (Nano-RPLC) was performed using
754 NanoElute2 systems (Bruker Daltonik, Bremen, Germany) and coupled to a timsTOF HT

755 mass spectrometer (Bruker Daltonik, Bremen, Germany) via a CaptiveSpray ion source.
756 The mobile phase consisted of solvent A (100% water, 0.1% formic acid) and solvent B
757 (100% acetonitrile, 0.1% formic acid).

758 Peptides were first loaded onto a C18 trap column (1 mm × 5 mm, ThermoFisher) before
759 being separated on an Aurora™ ULTIMATE analytical column (25 cm × 75 µm) packed
760 with 1.6 µm C18 particles (IonOpticks, Fitzroy, Australia) over a 60-minute gradient. The
761 flow rate was maintained at 250 nL/min, except for the final 7 minutes, where it was
762 increased to 400 nL/min. The gradient of mobile phase B was adjusted as follows: an
763 initial linear increase from 2% to 15% over 30 minutes, followed by a rise to 35% over 22
764 minutes, and a sharp increase to 85% within 0.5 minutes. The flow rate was then
765 adjusted to 400 nL/min in 0.5 minutes and held for 7 minutes to ensure complete
766 elution of hydrophobic peptides.

767 Data acquisition was performed in data-independent acquisition (DIA) mode using
768 parallel accumulation serial fragmentation (PASEF). Precursors with an m/z range of
769 350–1100 were analyzed across 12 MS/MS ramps in a cycle, with either two or three
770 quadrupole switches per ramp. Each cycle contained 30 MS/MS windows within a 0.65–
771 1.30 (1/k0) ion mobility range, using a fixed isolation window of 25 Da per step. The
772 acquisition time per DIA-PASEF ramp was set to 100 ms, resulting in a total cycle time of
773 approximately 1.38 seconds. Collision energy was ramped linearly from 65 eV at 1/k0 =
774 1.6 to 20 eV at 1/k0 = 0.6.

775 *Spectral deconvolution with DIA-NN*

776 DIA-NN 1.8.2[49] was used to process DIA-PASEF data in library-free mode. For the
777 TurboID and WT samples, each tissue and, in case of Adv^{Cre};$TurboID^{fl/fl}$ and $TurboID^{fl/fl}$
778 genotypes were processed in a separate analysis step using the same spectral library.
779 The spectral library was predicted from a Mus musculus proteome database from
780 UniProt containing 17,070 protein entries (downloaded on 2021-07-08), in case of the
781 TurboID samples it included in addition streptavidin (P22629|SAV_STRAV) and TurboID
782 sequence.[4] *In silico* digestion was performed using Trypsin/P, allowing up to two missed
783 cleavages. A maximum of three variable modifications was allowed per peptide
784 including methionine oxidation, and N-terminal acetylation, while Cysteine
785 carbamidomethylation was set as a fixed modification. Peptide length for the search
786 ranged from 5 to 52 amino acids. Precursor charge was set to 2-4. In accordance with
787 the DIA-PASEF acquisition method, the m/z ranges were set to 350–1100 for precursor
788 ions and 100–1700 for fragment ions. Mass accuracy was chosen automatically using
789 the first run in the experiment. Protein inference was performed using unique genes. For
790 neural network classifier the single-pass mode was chosen. Quantification was carried
791 out using RT-dependent cross-run normalization and the Quant UMS (high precision)
792 option. The main DIA-NN output was processed using the R package DiaNN to extract
793 MaxLFQ intensities[49,50] for all identified protein groups, applying a q-value threshold of

794 <0.01 at both the precursor and gene group levels. Matrices were merged by protein
795 group were applicable for downstream analyses.

796 *Neuronal protein enrichments*

797 Protein enrichments were calculated within each tissue/neuronal component prior to
798 merging. First, proteins were filtered for distinct gene symbols, keeping the first instance
799 where matches exist. Any protein detected in ≥75% of Adv^{Cre};$TurboID^{fl/fl}$ samples for a
800 given tissue, and no control sample was considered enriched (type "A"). This comprised
801 the majority of enrichments. For proteins in ≥75% of Adv^{Cre};$TurboID^{fl/fl}$ samples from any
802 tissue, and any amount of control underwent differential expression testing using a
803 standard limma framework (`lmFit` + `eBayes`).[51] Proteins were modelling by a
804 grouped factor for Tissue and TurboID Status, and contrasted within tissue between
805 TurboID and Control samples (ie. Paw.Turbo – Paw.Control). Proteins were considered
806 enriched when FDR < 0.05, and LFC > 1 ("DEP").

807 For explant analyses, we used the cross-tissue enrichments described above as a
808 reference for neuronal enrichment, instead of setting a 75% threshold (ie. explant data
809 were first filtered for neuronal enrichments using this reference list). Any proteins
810 detected in the turbo samples and not control (type "Specific"), as well as any proteins
811 that then hit a threshold of FDR < 0.05, and LFC > 1 (type "DEP") were considered
812 enriched in explant neurons.

813 *Pathway analyses*

814 GO enrichments were performed on enriched proteins and differentially expressed
815 proteins using the `enrichGO` function from the ClusterProfiler and org.Mm.eg.db
816 libraries in R[52]. Both cellular component (CC) and biological pathways (BP) were
817 extracted, with an adjusted p-value cutoff of 0.01 (Benjamini-Hochberg corrected). To
818 account for redundancy in the GO terms, outputs were slimmed using default settings:
819 `clusterProfiler::simplify(ego, cutoff=0.7, by="p.adjust", select_fun=min, measure =
820 'Wang')`.

821 For pathway analyses of TurboID-enriched proteins, a background of all proteins
822 detected across the four tissue wildtype whole cell lysates + proteins detected with
823 TurboID samples – this represents the entire universe of proteins which could have been
824 enriched in neurons using the TurboID approach. For pathway analyses of differentially
825 expressed proteins, a background of all proteins tested within the comparison was
826 used. For pathway analyses of co-expression modules (below), module genes were
827 compared to the universe of neuronal-enriched proteins.

828 *Subtype enrichment*

829 Neuronal subtype enrichment was calculated using an Overrepresentation Analysis
830 (ORA) on previously published custom-made gene lists from the mouse DRG
831 transcriptomics[13,14]. Briefly, custom gene enrichment lists for DRG neuronal subtypes

were calculated from Zheng et al. (2019) using DESeq2[14,53]. ORA was then performed on the neuronal enriched proteins from each tissue using ` Clusterprofiler ::enricher` [52]. For each tissue, the background was defined as any protein detected in whole cell lysate or TurboID samples, and the custom enrichment lists were filtered for proteins in the pre-defined background prior to ORA. ` Clusterprofiler ::enricher` does not allow the definition of both a custom background universe and custom gene set list (instead using only proteins defined in the custom gene sets as a background). To overcome this, the background proteins were defined as an additional gene set, and the gene set size was capped at 2000 to exclude this set from a direct enrichment analyses while maintaining them in the background. An FDR < 0.05 was considered significantly enriched, with an FDR =1 set for plotting.

Immune cell enrichment

The depletion of immune cells was determined by the "infiltration score" from the `ImmuCellAI` package (0.1.0), a GSEA-based approach to query immune signatures.[25] Protein names were converted to human gene symbols using the biomaRt package, and the expression of each tissue/compartment was presented against a background of all proteins detected in bulk and/or turbo samples, mirroring the pathway analysis (above). Missing values were imputed as zeros, and ImmuCellAI was run with default settings. The "infiltration score" was extracted from the resulting abundance matrix for plotting via ggplot2.

Sexual dimorphism

Male/Female differences were tested using a standard limma framework for the neuronal proteome of each tissue[51]. Proteins were modelled using a grouped factor for Tissue and Sex, and contrasted within Tissue as M – F. Proteins were considered enriched when FDR < 0.05, and abs(LFC > 1).

Weighted co-expression network analysis

A weighted protein co-expression network was built using the WGCNA package in R (version 1.72-5)[54]. Turbo samples were filtered for the entire universe of enriched proteins (ie., enriched in any component). Proteins expressed only in a single component and proteins with a variance of 0 were then removed, resulting in a matrix of 3142 proteins across 39 samples.

Soft power was established for a signed network using `pickSoftThreshold(type = "signed")` , with a model fit of 0.8. The scale-free topology fit index failed for reasonable powers (< 30), suggesting a strong correlation among large gene groups, thus violating the assumption of the scale-free topology approximation. As noted in the WGCNA package documentation, this is commonly seen with datasets containing multiple tissue types, and a lack of scale-free topology fit does not inherently invalidate the

data[54]. Consequently, we selected the recommended soft power of 14 for signed networks with 30-40 samples.

Network adjacency was calculated with ` adjacency(type = "signed")` and the topological overlap matrix was calculated with ` TOMsimilarity(TOMtype = "signed")` , both using default settings. Modules were established through adaptive branch pruning ` dynamicMods <- cutreeDynamic(dendro = geneTree, distM = dissTOM, deepSplit = 2, pamRespectsDendro = FALSE, minClusterSize = 30)` . Module eigengenes were then extracted for downstream analyses.

Terminal protein-protein interaction networks

Neuronally enriched proteins (the “neuronal proteome”) for each terminal compartment were used to generate large-scale protein-protein interaction networks in Cytoscape, via the stringApp[55,56]. For the peripheral terminals, a core cluster of 433 proteins were highly connected through high confidence (0.7) protein-protein interactions. For the central terminals, 2271 proteins formed the core cluster. For each compartment, these networks were then clustered further. Here, community clustering was performed on the resulting STRING network in Cytoscape, where the Girvan-Newman fast greedy algorithm was implemented through ClusterMaker2 via GLay[21,22]. Functional attributes within each cluster where then calculated via the stringApp, against a background of the entire peripheral/central terminal proteome respectively. Cluster numbers are somewhat arbitrary, but correspond to the supplemental table outputs with full enrichment details.

Oxaliplatin effects

The effects of the chemotherapy agent oxaliplatin on explant cultures was tested using limma.[51] For DRG explants dissected from wildtype mice, oxaliplatin was administered at 25 μM, 50 μM and 100 μM concentrations (or vehicle). Proteins here were modelled as Concentration.Condition, and contrasted within each concentration. For TurboID mice, data were first filtered for Turbo samples and neuronally-enriched proteins prior to modelling by Condition. In each case, limma was used to contrast by treatment condition (oxaliplatin – vehicle). Proteins were considered differentially expressed with FDR < 0.05, and abs(LFC) > 0.5. Downstream processing is described in the `*Pathway analyses*` section.

Comparisons against LFC and overall expression were compared to previously published, DIA-MS from *in vivo* oxaliplatin dosing by Yang *et al,* 2022.[27]

Rank-Rank Hypergeometric Overlap

Rank-Rank Hypergeometric Overlap (RRHO) testing was performed on limma outputs. Here, concordant and discordant gene profiles were calculated via the Stratified method using ranked ` -$\log_{10}$(p-values) * sign(effect size)` , implemented through the RRHO2 library in R in line with their published recommendations.[57]

907 *STRING analysis*

908 STRING protein-protein interaction analyses were performed through Cytoscape 3.10.3
909 using the stringApp.[55,56] A list of DEPs for each significant biological pathway were
910 extracted from the ClusterProfiler output (see: *Pathway analyses*) and loaded into the
911 stringApp with default settings. Proteins were coloured based on differential expression
912 in either TurboID only, or TurboID + bulk explant datasets.

913 *Immunohistochemistry (IHC)*

914 For IHC the tissue was dissected as above with modifications: instead of the dorsal part
915 of the SC, the whole L3-5 SC was taken out. The plantar paw punch contained not only
916 the epidermis and dermis but all layers below the bones. The dissected tissue was fixed
917 in 4% formalin/PBS for 3 h at 4°C, followed by overnight cryoprotection in 30% (w/v)
918 sucrose at 4°C. For sectioning, the tissue was embedded in Tissue-Tek O.C.T.
919 compound and frozen. Serial sections (SCN, DRG: 10 µm, SC: 30 µm, skin: 20-40 µm)
920 were obtained using a cryostat and mounted on SuperFrost Plus slides. Sections were
921 stored at -80°C until further processing.

922 Frozen sections were thawed at RT for 30 min before permeabilization and blocking in
923 0.4% Triton X-100/PBS containing 5% donkey serum for 30 min. Primary antibodies,
924 diluted in 0.1% Triton X-100/PBS with 1% donkey serum, were applied overnight at 4°C.
925 Following three washes in PBS, sections were incubated at RT for 2 h with Alexa Fluor-
926 conjugated secondary antibodies in PBS containing 1% donkey serum and 0.1% Triton
927 X-100. Unbound antibodies were removed by washing with PBS, and sections were
928 mounted using SlowFade™ Glass Soft-set Antifade Mountant Medium containing 4',6-
929 Diamidino-2-phenylindole (DAPI). Antibodies used are listed in STable 1.

930 *Graphics*

931 R base functions and the following libraries were used to compile plots unless
932 otherwise described: ggplot2, ggbiplot, ComplexHeatmap, cowplot. Figures and
933 schematics were designed in Inkscape.

934 *Use of generative AI*

935 Generative AI tools (OpenAI ChatGPT) were used solely to improve phrasing, clarity, and
936 formatting. All scientific concepts, experimental designs, hypotheses, and project goals
937 were developed by the research team. No synthetic or AI-generated data were included.

938

939
940
941

References

1. Middleton SJ, Barry AM, Comini M, et al. Studying human nociceptors: From fundamentals to clinic. *Brain*. 2021. doi:10.1093/brain/awab048
2. Qin W, Cho KF, Cavanagh PE, Ting AY. Deciphering molecular interactions by proximity labeling. *Nat Methods*. 2021;18(2). doi:10.1038/s41592-020-01010-5
3. Gingras AC, Abe KT, Raught B. Getting to know the neighborhood: using proximity-dependent biotinylation to characterize protein complexes and map organelles. *Curr Opin Chem Biol*. 2019;48. doi:10.1016/j.cbpa.2018.10.017
4. Branon TC, Bosch JA, Sanchez AD, et al. Efficient proximity labeling in living cells and organisms with TurboID. *Nat Biotechnol*. 2018;36(9). doi:10.1038/nbt.4201
5. Roux KJ, Kim DI, Raida M, Burke B. A promiscuous biotin ligase fusion protein identifies proximal and interacting proteins in mammalian cells. *J Cell Biol*. 2012;196(6). doi:10.1083/jcb.201112098
6. Dingar D, Kalkat M, Chan PK, et al. BioID identifies novel c-MYC interacting partners in cultured cells and xenograft tumors. *J Proteomics*. 2015;118. doi:10.1016/j.jprot.2014.09.029
7. May DG, Scott KL, Campos AR, Roux KJ. Comparative Application of BioID and TurboID for Protein-Proximity Biotinylation. *Cells*. 2020;9(5). doi:10.3390/cells9051070
8. Sunna S, Bowen C, Zeng H, et al. Cellular Proteomic Profiling Using Proximity Labeling by TurboID-NES in Microglial and Neuronal Cell Lines. *Mol Cell Proteomics*. 2023;22(6). doi:10.1016/j.mcpro.2023.100546
9. Rayaprolu S, Bitarafan S, Santiago J V., et al. Cell type-specific biotin labeling in vivo resolves regional neuronal and astrocyte proteomic differences in mouse brain. *Nat Commun*. 2022;13(1). doi:10.1038/s41467-022-30623-x
10. Hobson BD, Choi SJ, Mosharov E V., Soni RK, Sulzer D, Sims PA. Subcellular proteomics of dopamine neurons in the mouse brain. *Elife*. 2022;11. doi:10.7554/eLife.70921
11. Zurborg S, Piszczek A, Martínez C, et al. Generation and characterization of an Advillin-Cre driver mouse line. *Mol Pain*. 2011;7. doi:10.1186/1744-8069-7-66
12. Sisignano M, Baron R, Scholich K, Geisslinger G. Mechanism-based treatment for chemotherapy-induced peripheral neuropathic pain. *Nat Rev Neurol*. 2014;10(12). doi:10.1038/nrneurol.2014.211
13. Barry AM, Zhao N, Yang X, Bennett DL, Baskozos G. Deep RNA-seq of male and female murine sensory neuron subtypes after nerve injury. *Pain*. 2023;164(10):2196-2215. doi:10.1101/2022.11.21.516781
14. Zheng Y, Liu P, Bai L, Trimmer JS, Bean BP, Ginty DD. Deep Sequencing of Somatosensory Neurons Reveals Molecular Determinants of Intrinsic Physiological Properties. *Neuron*. 2019;103(4):598-616.e7. doi:10.1016/j.neuron.2019.05.039
15. Lopes DM, Denk F, McMahon SB. The Molecular Fingerprint of Dorsal Root and Trigeminal Ganglion Neurons. *Front Mol Neurosci*. 2017. doi:10.3389/fnmol.2017.00304
16. Sun X, Sun H, Han X, et al. Deep Single-Cell-Type Proteome Profiling of Mouse Brain by Nonsurgical AAV-Mediated Proximity Labeling. *Anal Chem*. 2022;94(13). doi:10.1021/acs.analchem.1c05212
17. Dumrongprechachan V, Salisbury RB, Soto G, Kumar M, MacDonald ML, Kozorovitskiy Y. Cell-type and subcellular compartment-specific APEX2 proximity labeling reveals activity-dependent nuclear proteome dynamics in the striatum. *Nat Commun*. 2021;12(1). doi:10.1038/s41467-021-25144-y
18. Bhuiyan SA, Xu M, Yang L, et al. Harmonized cross-species cell atlases of trigeminal and dorsal root ganglia. *Sci Adv*. 2024;10(25). doi:10.1126/sciadv.adj9173
19. Tavares-Ferreira D, Shiers S, Ray PR, et al. Spatial transcriptomics of dorsal root ganglia identifies molecular signatures of human nociceptors. *Sci Transl Med*. 2022;14(632):eabj8186. doi:DOI: 10.1126/scitranslmed.abj8186
20. Szklarczyk D, Gable AL, Nastou KC, et al. The STRING database in 2021: customizable

protein–protein networks, and functional characterization of user-uploaded gene/measurement sets. *Nucleic Acids Res*. 2021;49(D1):D605. doi:10.1093/NAR/GKAA1074

21. Utriainen M, Morris JH. clusterMaker2: a major update to clusterMaker, a multi-algorithm clustering app for Cytoscape. *BMC Bioinformatics*. 2023;24(1). doi:10.1186/s12859-023-05225-z
22. Su G, Kuchinsky A, Morris JH, States DJ, Meng F. GLay: Community structure analysis of biological networks. *Bioinformatics*. 2010;26(24). doi:10.1093/bioinformatics/btq596
23. Xian F, Sondermann JR, Varela DG, Schmidt M. Deep proteome profiling reveals signatures of age and sex differences in paw skin and sciatic nerve of naïve mice. *Elife*. 2022;11. doi:10.7554/eLife.81431
24. Barry AM, Sondermann JR, Sondermann J-H, Gomez-Varela D, Schmidt M. Region-resolved quantitative proteome profiling reveals molecular dynamics associated with chronic pain in the PNS and spinal cord. *Front Mol Neurosci*. 2018;11(August):259. doi:10.3389/fnmol.2018.00259
25. Miao YR, Xia M, Luo M, Luo T, Yang M, Guo AY. ImmuCellAI-mouse: a tool for comprehensive prediction of mouse immune cell abundance and immune microenvironment depiction. *Bioinformatics*. 2022;38(3). doi:10.1093/bioinformatics/btab711
26. Dyring-Andersen B, Løvendorf MB, Coscia F, et al. Spatially and cell-type resolved quantitative proteomic atlas of healthy human skin. *Nat Commun*. 2020;11(1). doi:10.1038/s41467-020-19383-8
27. Yang L, Wang H, Lu W, et al. Quantitative proteomic analysis of oxaliplatin induced peripheral neurotoxicity. *J Proteomics*. 2022;266. doi:10.1016/j.jprot.2022.104682
28. Matzinger M, Mayer RL, Mechtler K. Label-free single cell proteomics utilizing ultrafast LC and MS instrumentation: A valuable complementary technique to multiplexing. *Proteomics*. 2023;23(13-14). doi:10.1002/pmic.202200162
29. Grindberg R V., Yee-Greenbaum JL, McConnell MJ, et al. RNA-sequencing from single nuclei. *Proc Natl Acad Sci*. 2013;110(49):19802-19807. doi:10.1073/pnas.1319700110
30. Ferreira DT, Shen BQ, Mwirigi JM, et al. Deciphering the molecular landscape of human peripheral nerves: implications for diabetic peripheral neuropathy. *bioRxiv*. 2024:2024.06.15.599167. https://www.biorxiv.org/content/10.1101/2024.06.15.599167v1%0Ahttps://www.biorxiv.org/content/10.1101/2024.06.15.599167v1.abstract.
31. North RY, Li Y, Ray P, et al. Electrophysiological and transcriptomic correlates of neuropathic pain in human dorsal root ganglion neurons. *Brain*. 2019;142(5):1215-1226. doi:10.1093/brain/awz063
32. Schulte RR, Ho RH. Organic anion transporting polypeptides: Emerging roles in cancer pharmacology. *Mol Pharmacol*. 2019;95(5). doi:10.1124/mol.118.114314
33. Litke C, Hagenston AM, Kenkel AK, et al. Organic anion transporter 1 is an HDAC4-regulated mediator of nociceptive hypersensitivity in mice. *Nat Commun*. 2022;13(1). doi:10.1038/s41467-022-28357-x
34. Huang KM, Leblanc AF, Uddin ME, et al. Neuronal uptake transporters contribute to oxaliplatin neurotoxicity in mice. *J Clin Invest*. 2020;130(9). doi:10.1172/JCI136796
35. Filipski KK, Mathijssen RH, Mikkelsen TS, Schinkel AH, Sparreboom A. Contribution of organic cation transporter 2 (OCT2) to cisplatin-induced nephrotoxicity. *Clin Pharmacol Ther*. 2009;86(4). doi:10.1038/clpt.2009.139
36. Sprowl JA, Ciarimboli G, Lancaster CS, et al. Oxaliplatin-induced neurotoxicity is dependent on the organic cation transporter OCT2. *Proc Natl Acad Sci U S A*. 2013;110(27). doi:10.1073/pnas.1305321110
37. Li Y, Drabison T, Nepal M, et al. Targeting a xenobiotic transporter to ameliorate vincristine-induced sensory neuropathy. *JCI Insight*. 2023;8(14).

doi:10.1172/jci.insight.164646
38. Leskelä S, Jara C, Leandro-García LJ, et al. Polymorphisms in cytochromes P450 2C8 and 3A5 are associated with paclitaxel neurotoxicity. *Pharmacogenomics J*. 2011;11(2). doi:10.1038/tpj.2010.13
39. Schmidt D, Díaz P, Muñoz D, et al. Characterisation of the pathophysiology of neuropathy and sensory dysfunction in a mouse model of recessive dystrophic epidermolysis bullosa. *Pain*. 2022;163(10). doi:10.1097/j.pain.0000000000002599
40. Cooper AH, Barry AM, Chrysostomidou P, et al. Peripheral nerve injury results in a biased loss of sensory neuron subpopulations. *Pain*. August 2024. doi:10.1097/j.pain.0000000000003321
41. Perez-Riverol Y, Bai J, Bandla C, et al. The PRIDE database resources in 2022: A hub for mass spectrometry-based proteomics evidences. *Nucleic Acids Res*. 2022;50(D1). doi:10.1093/nar/gkab1038
42. Tycko J, Wainberg M, Marinov GK, et al. Mitigation of off-target toxicity in CRISPR-Cas9 screens for essential non-coding elements. *Nat Commun*. 2019;10(1). doi:10.1038/s41467-019-11955-7
43. Doench JG, Fusi N, Sullender M, et al. Optimized sgRNA design to maximize activity and minimize off-target effects of CRISPR-Cas9. *Nat Biotechnol*. 2016;34(2). doi:10.1038/nbt.3437
44. Madisen L, Zwingman TA, Sunkin SM, et al. A robust and high-throughput Cre reporting and characterization system for the whole mouse brain. *Nat Neurosci*. 2010;13(1):133-140. doi:10.1038/NN.2467
45. Concordet JP, Haeussler M. CRISPOR: Intuitive guide selection for CRISPR/Cas9 genome editing experiments and screens. *Nucleic Acids Res*. 2018;46(W1). doi:10.1093/nar/gky354
46. Haeussler M, Schönig K, Eckert H, et al. Evaluation of off-target and on-target scoring algorithms and integration into the guide RNA selection tool CRISPOR. *Genome Biol*. 2016;17(1). doi:10.1186/s13059-016-1012-2
47. Livni L, Lees JG, Barkl-Luke ME, Goldstein D, Moalem-Taylor G. Dorsal root ganglion explants derived from chemotherapy-treated mice have reduced neurite outgrowth in culture. *Neurosci Lett*. 2019;694. doi:10.1016/j.neulet.2018.11.016
48. Hughes CS, Moggridge S, Müller T, Sorensen PH, Morin GB, Krijgsveld J. Single-pot, solid-phase-enhanced sample preparation for proteomics experiments. *Nat Protoc*. 2019;14(1). doi:10.1038/s41596-018-0082-x
49. Demichev V, Messner CB, Vernardis SI, Lilley KS, Ralser M. DIA-NN: neural networks and interference correction enable deep proteome coverage in high throughput. *Nat Methods*. 2020;17(1). doi:10.1038/s41592-019-0638-x
50. Cox J, Hein MY, Luber CA, Paron I, Nagaraj N, Mann M. Accurate proteome-wide label-free quantification by delayed normalization and maximal peptide ratio extraction, termed MaxLFQ. *Mol Cell Proteomics*. 2014;13(9). doi:10.1074/mcp.M113.031591
51. Ritchie ME, Phipson B, Wu D, et al. Limma powers differential expression analyses for RNA-sequencing and microarray studies. *Nucleic Acids Res*. 2015;43(7). doi:10.1093/nar/gkv007
52. Wu T, Hu E, Xu S, et al. clusterProfiler 4.0: A universal enrichment tool for interpreting omics data. *Innov*. 2021;2(3):100141. doi:10.1016/J.XINN.2021.100141
53. Love MI, Huber W, Anders S. Moderated estimation of fold change and dispersion for RNA-seq data with DESeq2. *Genome Biol 2014 1512*. 2014;15(12):1-21. doi:10.1186/S13059-014-0550-8
54. Langfelder P, Horvath S. WGCNA: An R package for weighted correlation network analysis. *BMC Bioinformatics*. 2008;9. doi:10.1186/1471-2105-9-559
55. Doncheva NT, Morris JH, Holze H, et al. Cytoscape stringApp 2.0: Analysis and Visualization of Heterogeneous Biological Networks. *J Proteome Res*. 2023;22(2).

doi:10.1021/acs.jproteome.2c00651
56. Shannon P, Markiel A, Ozier O, et al. Cytoscape: A software Environment for integrated models of biomolecular interaction networks. *Genome Res*. 2003;13(11). doi:10.1101/gr.1239303
57. Cahill KM, Huo Z, Tseng GC, Logan RW, Seney ML. Improved identification of concordant and discordant gene expression signatures using an updated rank-rank hypergeometric overlap approach. *Sci Rep*. 2018;8(1). doi:10.1038/s41598-018-27903-2

1108 **Supplemental Tables + Figures: Proximity labelling reveals the compartmental**
1109 **proteome of murine sensory neurons**
1110
1111

Order	*Content*
Supplemental Table 1	expression matrix, TurboID (compartments)
Supplemental Table 2	neuronal enrichment
Supplemental Table 3	subtype enrichment
Supplemental Table 4	sexual dimorphism
Supplemental Table 5	GO compartment functions
Supplemental Table 6	WGCNA functions
Supplemental Table 7	PPI peripheral terminal functions
Supplemental Table 8	PPI central terminal functions
Supplemental Table 9	expression matrix, bulk (tissues)
Supplemental Table 10	TurboID unique proteins
Supplemental Table 11	expression matrix, explant (bulk)
Supplemental Table 12	DEPs (bulk oxaliplatin)
Supplemental Table 13	expression matrix, explant (TurboID)
Supplemental Table 14	neuronal enrichment, explant
Supplemental Table 15	DEPs (TurboID oxaliplatin)
Supplemental Table 16	GO oxaliplatin treated-explant functions
Supplemental Table 17	Key resources

1112
1113
1114
1115 **Supplemental Table 17**. Key Resources

Type	Designation	Source	Identifiers	Additional
Mouse strain	C57BL/6J	In house bred		Wild type, male
Mouse strain	Advillin^{Cre}	Kind gift of Prof. Dr. Klaus-Armin Nave, MPIEM, Göttingen	(Zurborg et al., 2011) Tg(Avil-cre)1Phep MGI:5292346	
Mouse strain	TurboID$^{fl/fl}$	Current study	ROSA26$^{em1(TurboID)Bros}$	
Chemical	Acetonitrile	Fisher Scientific	10001334	
Chemical	Formic Acid	Fisher Scientific	15658430	
Chemical	10x PBS	Fisher Scientific	11594516	
Chemical	Tris 1M	Accugene/Avantor	51237	
Chemical	NaCl, 5M	Accugene/Avantor	51202	
Chemical	Triton™ X-100	Fisher Scientific	10102913	

Chemical	Invitrogen™ SDS, 20% Solution, RNase-free	Fisher Scientific	AM9820	
Chemical	Biotin	Sigma-Aldrich	B4501-10G	
Chemical	Oxaliplatin	Sigma-Aldrich	O9512-5MG	
Chemical	Glycerol	Fisher Scientific	10021083	
Chemical	Dithiothreitol 1M	Sigma-Aldrich	43816	
Chemical	Acetone	Sigma-Aldrich	1000201000	
Chemical	Ethanol	Sigma-Aldrich	1117272500	
Chemical	Iodoacetamide	Sigma-Aldrich	I1149	
Chemical	Ammonium bicarbonate	Sigma-Aldrich	09830-500G	
Chemical	Water MS grade	Sigma-Aldrich	1.15333.1000	
other	Trypsin/Lys-C	Promega	V5073	
other	rhβ-Nerve Growth Factor	R&D Systems	256-GF	
other	Gibco™ DMEM/F-12, GlutaMAX™ Supplement	Fisher Scientific	31331028	
other	Sera-Mag SpeedBead beads	Cytiva	65152105050250, 45152105050250	1:1 mix
other	Sera-Mag SpeedBead Blocked Streptavidin Particles	Cytiva	21152104010150	
other	Complete protease inhibitor cocktail	Roche/ Merck	58929700001	Mix of protease inhibitors
other	Protein LoBind tube	Eppendorf	0030108116, 0030108132	Reagent tube
other	4X Bolt™ LDS sample buffer	Fisher Scientific	B0007	
other	10X Bolt™ Sample Reducing Agent	Fisher Scientific	B0009	
other	Bolt™ Bis-Tris Plus Mini Protein Gels, 4-12%, 1.0 mm	Fisher Scientific	NW04120BOX	
other	Invitrogen™ iBlot™ 2 Transfer Stacks, PVDF, mini	Fisher Scientific	IB24002	
other	SlowFade™ Glass Soft-set Antifade Mountant, with DAPI	Fisher Scientific	S36920	

other	Aurora Series UHPLC column	IonOpticks	AUR2-25075C18A-CSI	
other	Biopsy punch 4mm	Kai medical	48401	
antibody	Streptavidin-AF680	invitrogen	S21378	1:500 dilution
antibody	Mouse mc α-β-actin	Sigma-Aldrich	A1978-200UL	1:500 dilution
antibody	Streptavidin-AF555	Invitrogen	S32355	1:500 dilution
antibody	Rabbit α-NF200	Sigma-Aldrich	N4142-25UL	1:500 dilution
antibody	Chicken α-Peripherin	ABcam	AB39374	1:100 dilution
antibody	Donkey α-mouse AF790	Invitrogen	A11371	1:8000 dilution
antibody	Donkey α-rabbit 488	Invitrogen	A-21206	1:250 dilution
antibody	Donkey α-chicken 647	Invitrogen	A78952	1:250 dilution
software, algorithm	DIA-NN	https://github.com/vdemichev/DiaNN		1.8.2
software, algorithm	R	https://www.r-project.org/		4.3.2
software, algorithm	Mouse proteome	Uniprot	UP000000589	
software, algorithm	Cytoscape	https://cytoscape.org/		3.10.3

1118 **Supplemental Figures**

1119

1120

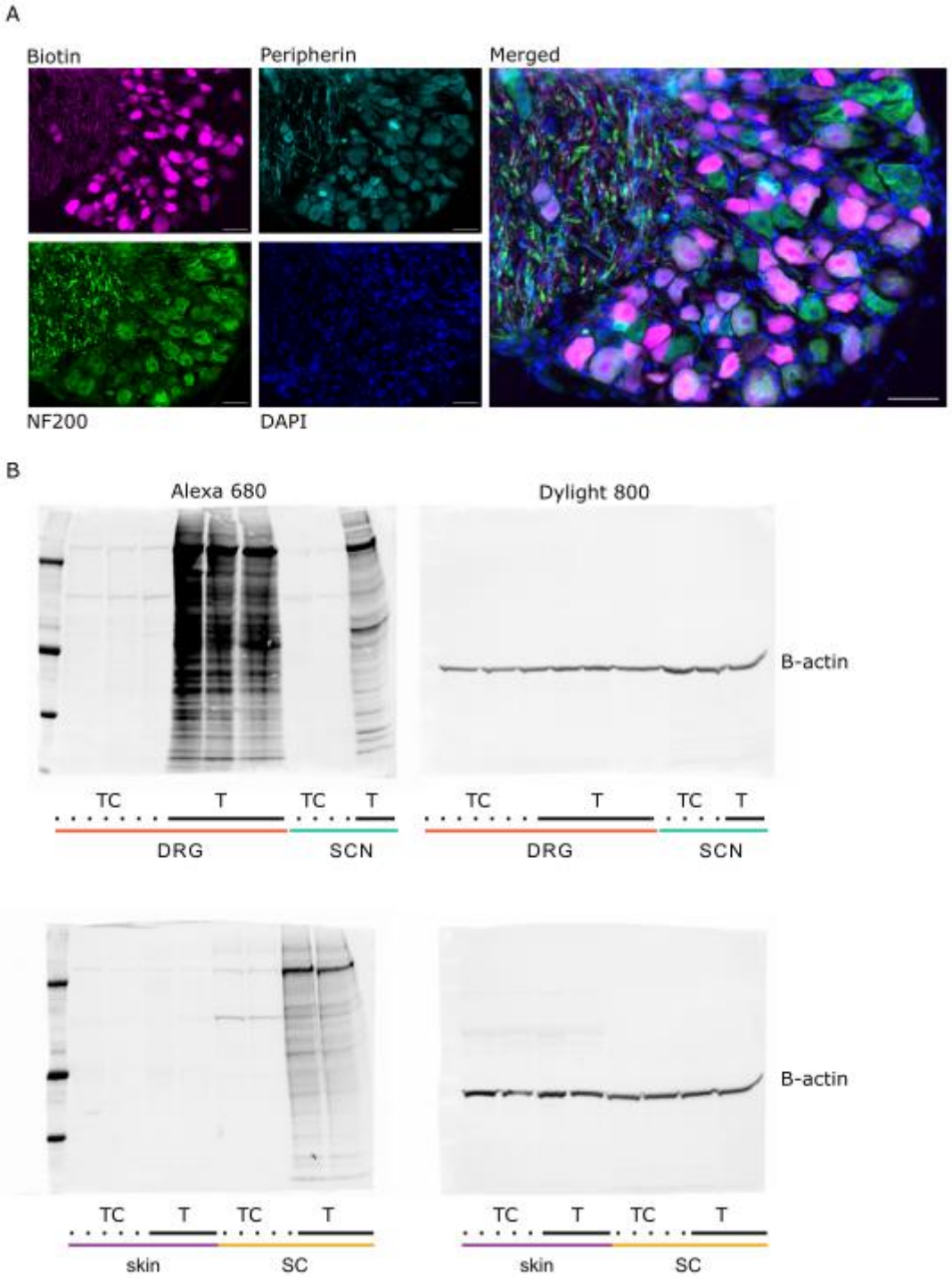

1121

1122 **Supplemental Figure 1.** A. Immunohistochemistry of Adv^{Cre};TurboID$^{fl/fl}$ with classic sensory
1123 neuron markers peripherin and NF200. Scale bar = 50 um. B. Western Blot analyses for TurboID
1124 (left) and B-actin loading controls (right). Adv^{Cre};TurboID$^{fl/fl}$ (T) and TurboID$^{fl/fl}$ (TC) samples for
1125 each tissue were loaded. DRG, dorsal root ganglia; SCN, sciatic nerve; SC, lumbar spinal cord.

1126

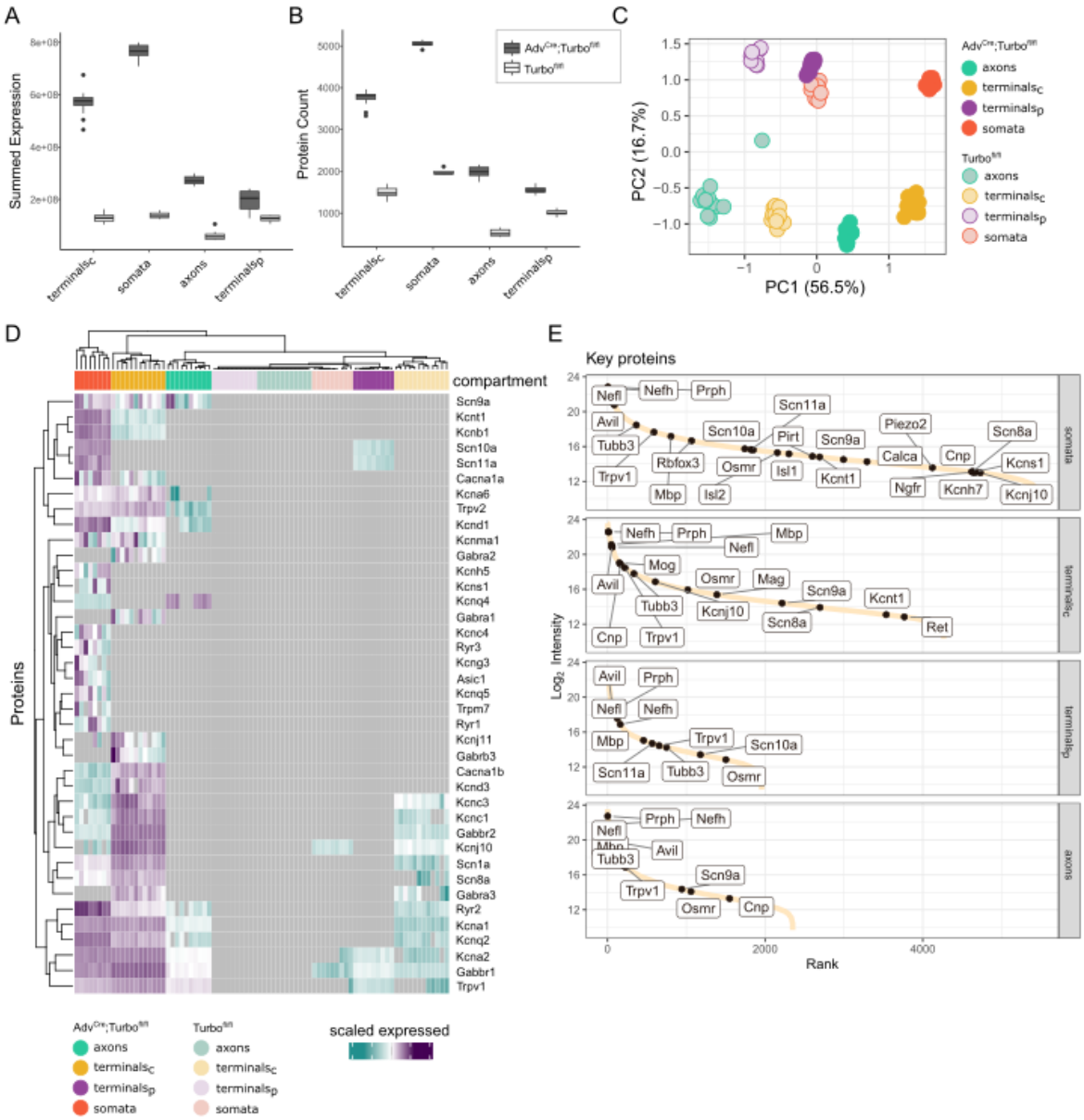

Supplemental Figure 2. DIA-PASEF mass spectrometry of TurboID and control samples across sensory neuron compartments. A-B. Summed expression (A), and Protein Group counts (B) by tissue and TurboID status. C. PCA across all samples. D. Heatmap of ion channel expression across all samples. E. Dynamic range for proteins of interest in the Adv^{Cre};TurboID$^{fl/fl}$, plotted as expression (log_2 Intensity) per component. terminals$_p$ = peripheral terminals (skin); terminals$_c$ = central terminals (SC). Relates to Figure 2.

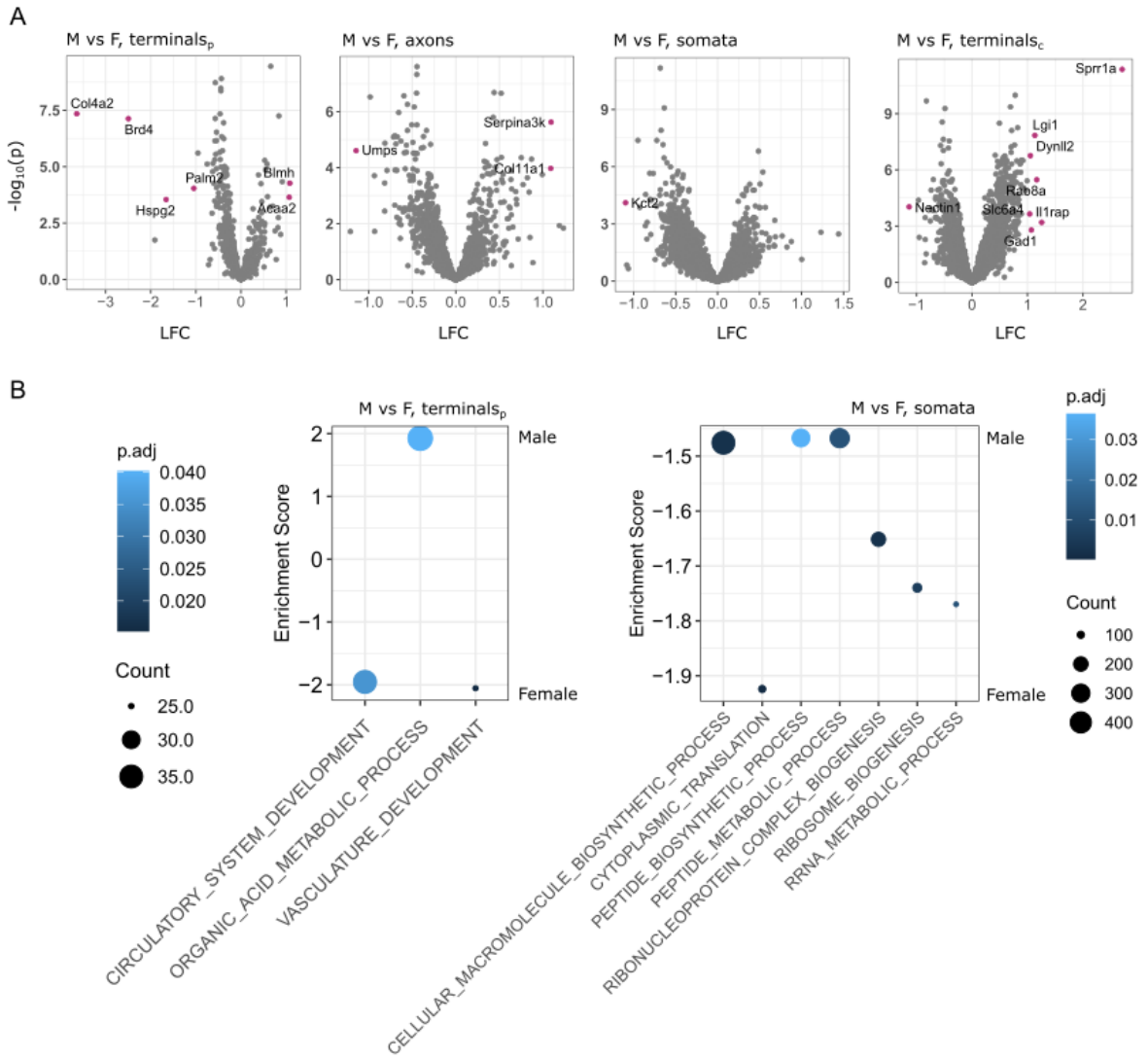

Supplemental Figure 3. Sexual dimorphism across neuronal compartments. A. Differential protein expression by component, comparing male vs female mice within TurboID samples enriched for the neuronal proteome. Significant proteins are in pink. LFC = $\log_2$ fold change B. Biological Pathway analysis for the paw and DRG on ranked fold changes between male and female samples. Counts reflect the number of proteins in each respective term. terminals$_p$ = peripheral terminals; terminals$_c$ = central terminals.

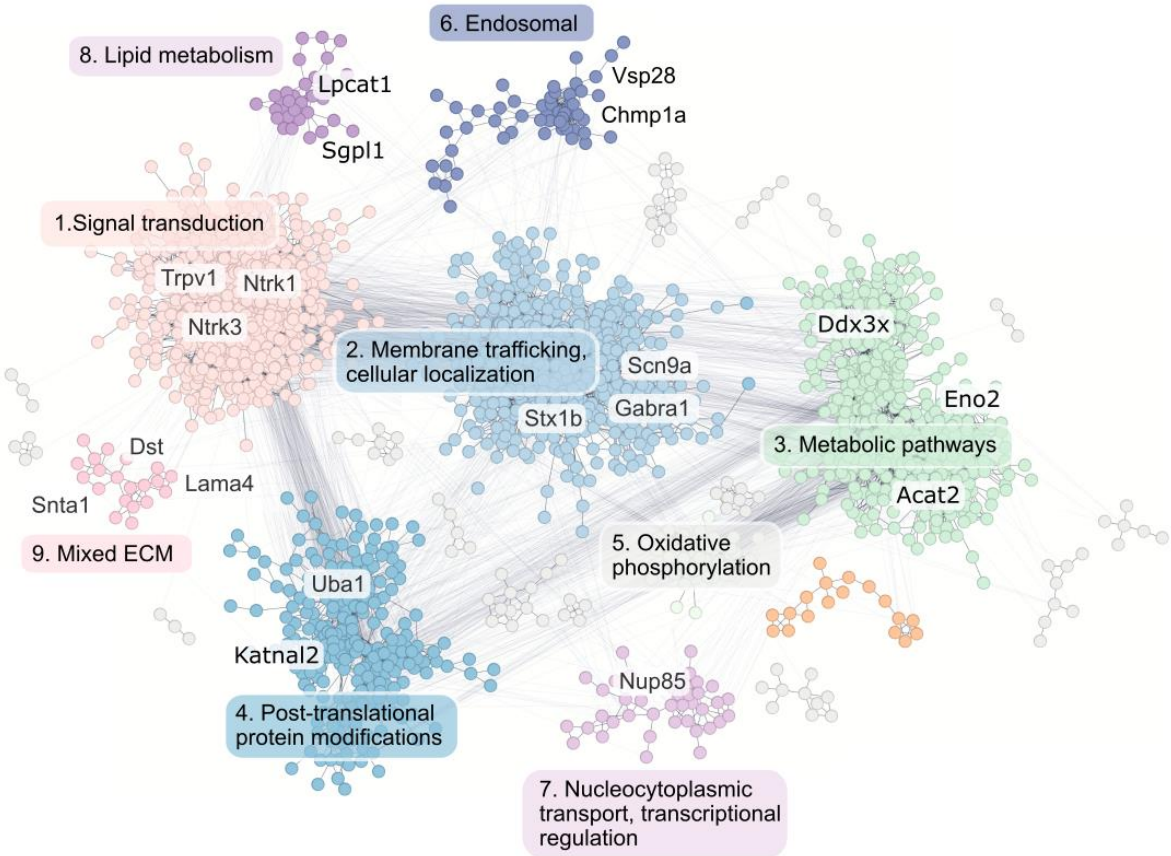

Supplemental Figure 4. Community clustering of the central terminal proteome, with edges denoting high confidence protein-protein interactions. Protein nodes are coloured by cluster, and clusters are described by functional summaries with proteins of interest highlighted. Full functional enrichments are available at Stable 8.

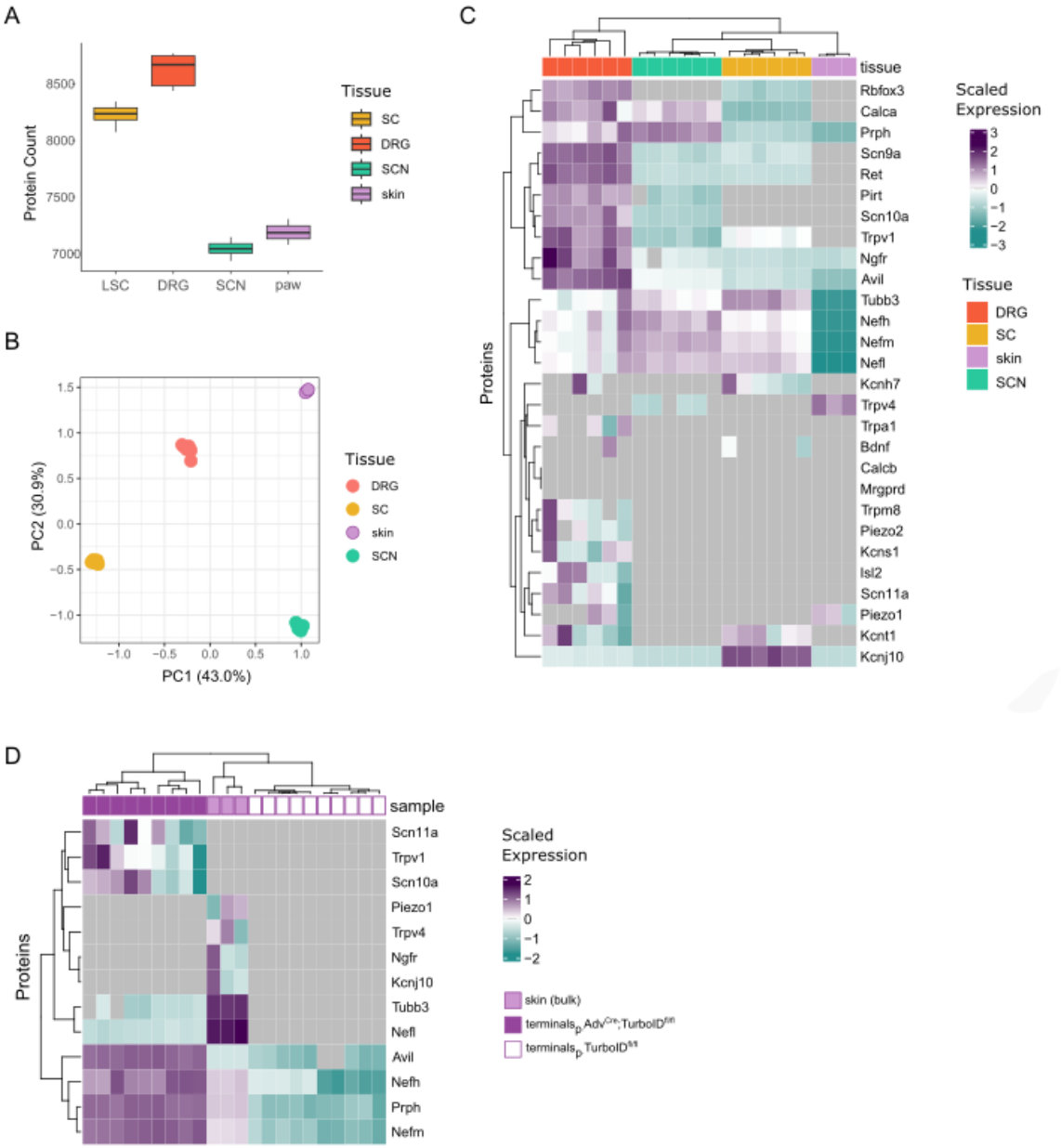

Supplemental Figure 5. DIA-PASEF tissue proteomes along the peripheral somatosensory axis. A. Protein Group (PG) counts per tissue. B. PCA by tissue. C. Heatmap of key neuronal genes. D. Comparison between TurboID and wildtype, whole tissue (WT) proteomes for key neuronal proteins.

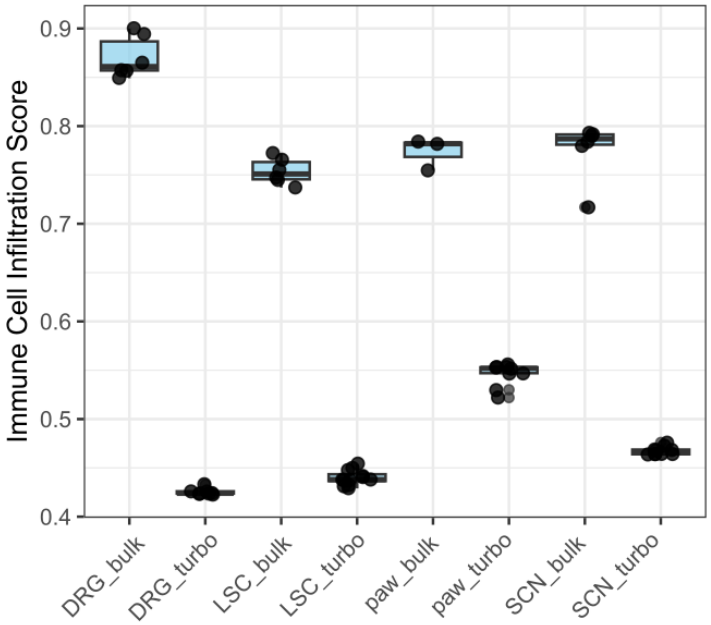

Supplemental Figure 6. Depletion of ImmuCellAI immune cell signatures between bulk (WT) and turbo (Adv^{Cre};Turbo$^{fl/fl}$) samples for each tissue/compartment.

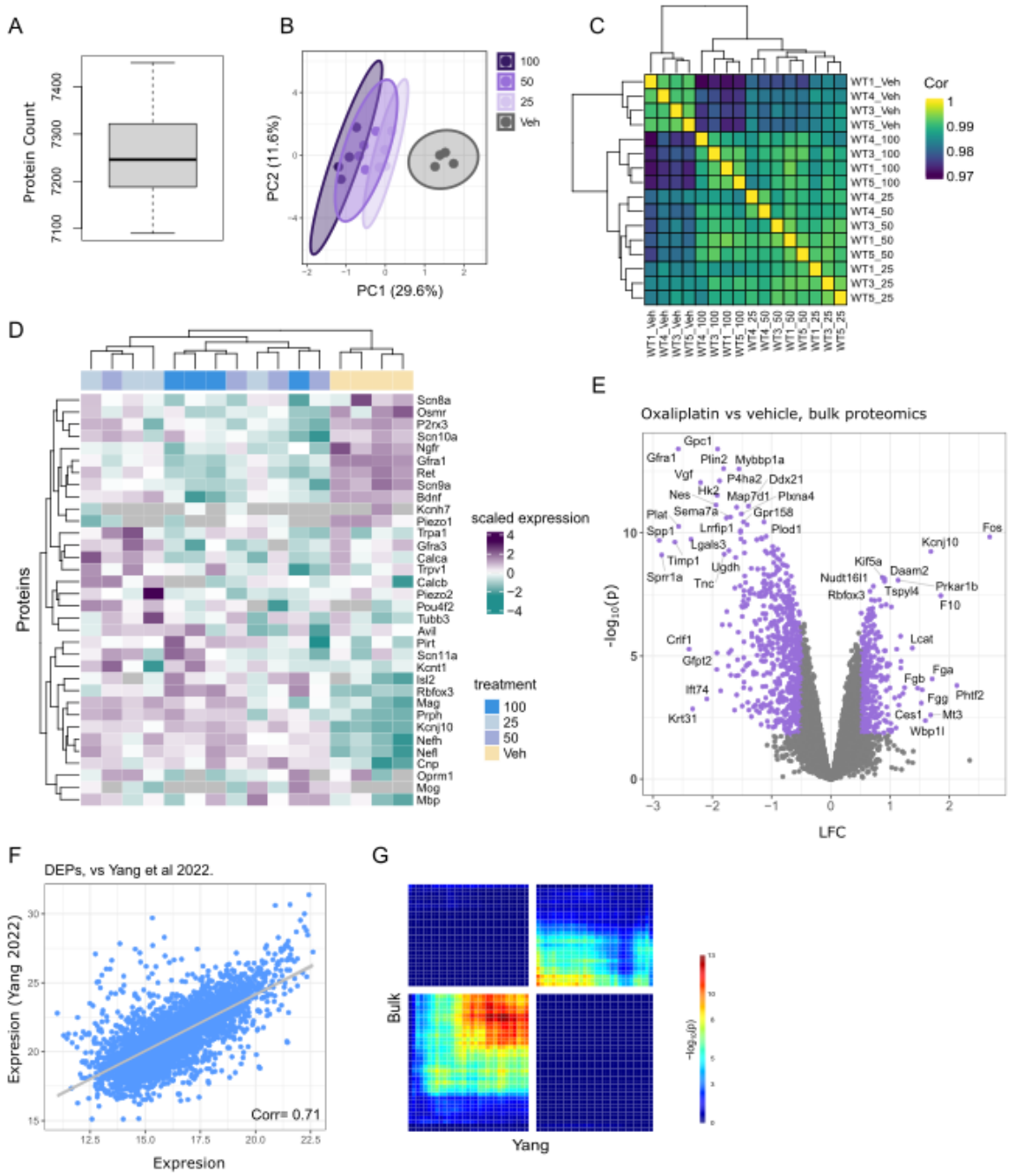

Supplemental Figure 7. DIA-PASEF proteomics of DRG explants exposed to Oxaliplatin (25, 50 or 100 uM) or Vehicle (Veh). A. Protein Group counts. B. PCA across sample conditions. C. Correlation across samples, labelled as Oxaliplatin (25, 50, 100) or Vehicle (Veh). D. Heatmap across key neuronal proteins. E. Differentially expressed proteins between 100 uM Oxaliplatin and Vehicle-treated DRG explants. Purple dots are significant (FDR < 0.05, LFC > 0.5). F. Correlation of protein expression with previously published, *in vivo* treated DRGs (Yang et al., 2022). Rank-rank hypergeometric overlap between oxaliplatin changes across datasets (Yang et al., 2022 and here). DEP, differentially expressed proteins; LFC, $\log_2$ fold change.

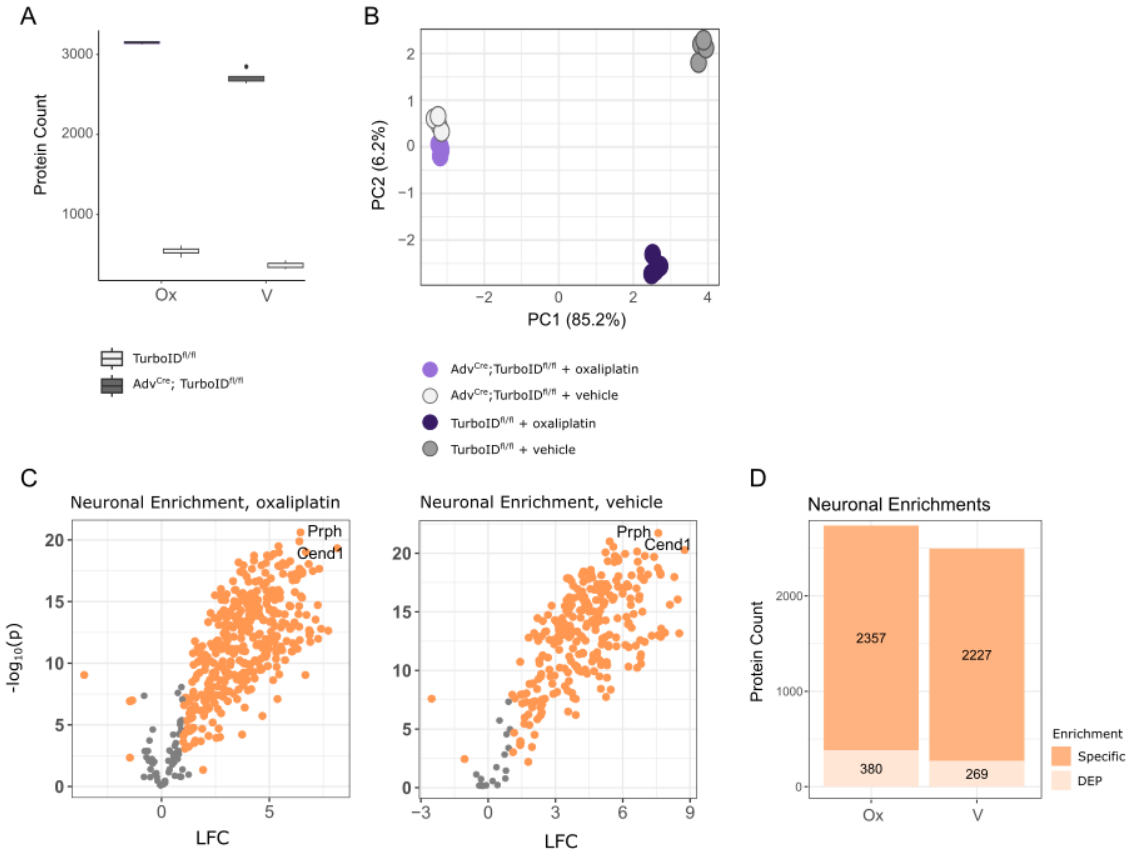

Supplemental Figure 8. DIA-PASEF proteomics of DRG explants from Adv^{Cre};TurboID$^{fl/fl}$ and TurboID$^{fl/fl}$ mice. A. Protein group counts across conditions, before neuronal enrichment. B. PCA across explant samples. C. Differentially expressed proteins between Adv^{Cre};TurboID$^{fl/fl}$ and TurboID$^{fl/fl}$ explant samples, for both vehicle and oxaliplatin-treated cultures. D. Neuronal enrichments for each condition. LFC = $\log_2$ fold change. Ox = oxaliplatin. V = vehicle.

1185 **Supplemental Methods: Proximity labelling reveals the compartmental proteome of**
1186 **murine sensory neurons**

1187

1188 *Generation of TurboID mutant mice using CRISPR/Cas9*

1189 The conditional TurboID knock-in (cKI) mouse line was generated by site-directed CRISPR/Cas9
1190 mutagenesis in the ROSA26 locus. Superovulated C57Bl6/J females were mated with C57Bl6/J
1191 males and fertilized eggs collected. In-house produced CRISPR reagents (hCas9_mRNA,
1192 sgRNAs, preformed Cas9_sgRNA-RNP complexes and the homology-directed repair fragment
1193 (HDR fragment)) were microinjected into the pronucleus and the cytoplasm of pronuclear-stage
1194 zygotes using an Eppendorf Femtojet. Importantly, all nucleotide-based CRISPR/Cas9 reagents
1195 (sgRNAs and hCAS9_mRNA) were used as RNA molecules and were not plasmid-encoded,
1196 reducing the probability of off-target effects due to the short lifetime of RNA-based reagents
1197 (Tycko et al., 2019; Doench et al., 2016). The TurboID-containing HDR fragment was generated
1198 by subcloning a V5-tag-TurboID sequence into the Ai14-ROSA26-based plasmid backbone
1199 (Madisen et al., 2010) and isolated as a linear DNA fragment by SacI/AgeI restriction enzyme
1200 double digestion. Two sgRNAs targeting the ROSA26 Locus were selected using the guide RNA
1201 selection tool CRISPOR (Haeussler et al, 2016; Concordet & Haeussler, 2018). The correct
1202 locus-specific insertion of the HDR fragment was confirmed by localization PCRs with primers
1203 upstream and downstream of the HDR sequence.

1204

1205 *Genotyping Strategy*

1206 For genotyping, genomic DNA (gDNA) was isolated from tail biopsies using a genomic DNA
1207 isolation kit (Nexttec, #10.924). For the location PCRs, 20 µL reactions were prepared using 1 µL
1208 clean gDNA (15-80ng), 4 µL PrimerSet (4 pmol final each), 4 µL 5X Reaction Buffer (Finnzymes
1209 #F-524), 0.4 µL PhireHot-Start II Taq DNA Polymerase (Finnzymes #F-122L), 1 µL 10 mM dNTPs
1210 (Bioline #DM-515107), 4 µL Hi-Spec Additive (Bioline #HS-014101) and 5.6 µL H2O.
1211 Thermocycler parameters location-PCR Rosa26 left arm: 98°C for 5 min, (98 °C for 45 s, 64 °C
1212 for 30 s, 72 °C for 60 s) repeated for 34 cycles, final step at 72 °C for 10 min. Thermocycler
1213 parameters-location PCR Rosa26 right arm: 98°C for 5 min, (98 °C for 45 s, 68 °C for 30 s, 72 °C
1214 for 180 s) repeated for 34 cycles, final step at 72 °C for 10 min.

1215

1216 For the diagnostic routine genotyping PCR, 20 µL reactions were prepared using 1 µL clean
1217 gDNA (15-80ng), 4 µL PrimerSet (4 pmol final each), 4 µL 5X Reaction Buffer (Biozym
1218 #331620XL), 0.2 µL Hot-Start Taq DNA Polymerase (Biozym #331620XL), 1 µL 50 mM MgCl2
1219 (AGCTLab stock) and 9.8 µL H2O. Thermocycler parameters: 96°C for 3 min, (94 °C for 30 s, 62
1220 °C for 60 s, 72 °C for 60 s) repeated for 32 cycles, final step at 72 °C for 7 min.

1221

1222 *Rosa26 Locus sgRNAs*
1223 Sense Rosa26 protospacer-sgRNA1 sequence: 5‘-ACTCCAGTCTTTCTAGAAGA-3‘ (PAM = TGG)
1224 Antisense Rosa26 protospacer-sgRNA2 sequence: 5‘-CGCCCATCTTCTAGAAAGAC-3‘ (PAM =
1225 TGG)

C57BL6J_Chrom6_Rosa26 target locus (insertion site):

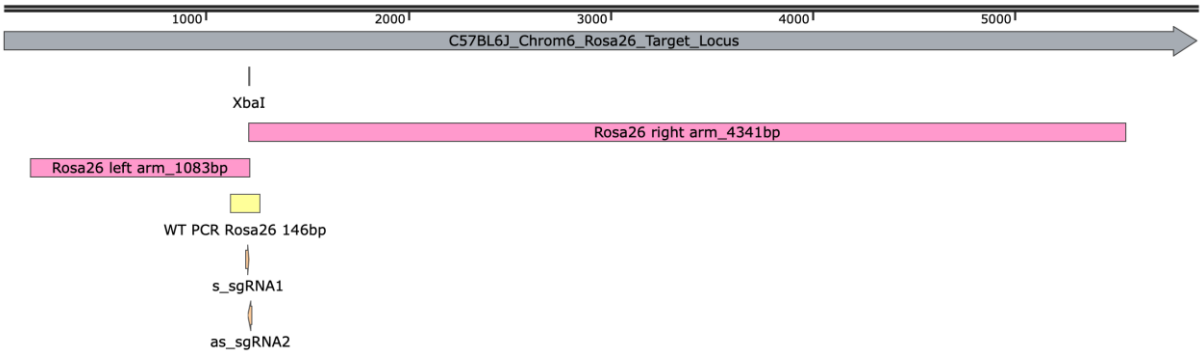

Ai14-TurboID_Rosa26 HDR fragment targeting strategy (conditional knock-in)

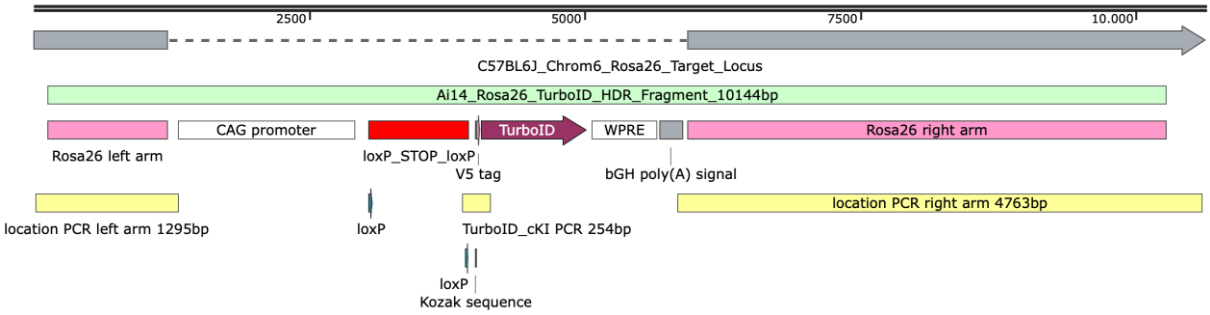

Ai14-TurboID_Rosa26 Cre recombined (knock-in)

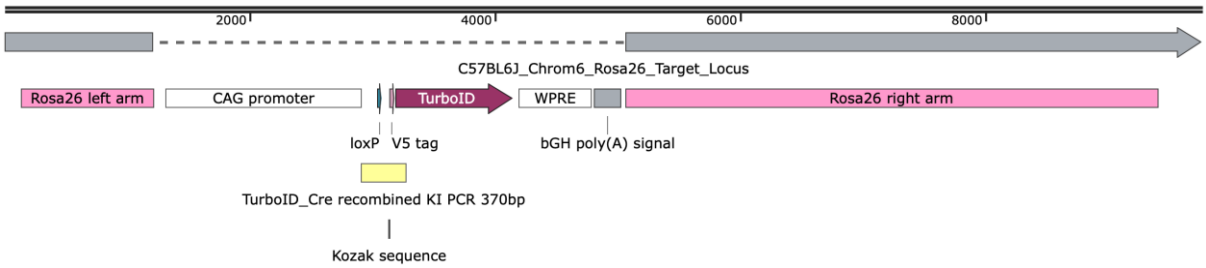

SMethods, Figure1. Schematic representation of the target locus, the targeting strategy (HDR fragment) and the Cre recombination event.

Ai14-TurboID_Rosa26 HDR fragment and sequence annotations:

Lower case letters = upstream and downstream HDR fragment ROSA26 sequences

Capital letters = HDR fragment after locus-specific insertion

Magenta = ROSA26 left- and right arm sequence
Blue = CAG-promoter
Red BOLD = loxP sites
Underlined BOLD = loxP flanked STOP cassette
Green BOLD = ATG Start- and TAA Stop codon
Brown BOLD = V5-tag
Purple BOLD = TurboID
Black BOLD = WPRE
Black underlined = bGH poly(A) signal

5’-
ggaggctgccggggccgcctaaagaagaggctgtgctttggggctccggctcctcagagagcctcggctaggtaggggatcgggactctggcggg
agggcggcttggtgcgtttgcggggatgggcggccGCGGCAGGCCCTCCGAGCGTGGTGGAGCCGTTCTGTGAGACAGC
CGGGTACGAGTCGTGACGCTGGAAGGGGCAAGCGGGTGGTGGGCAGGAATGCGGTCCGCCCTGCAGCAA
CCGGAGGGGGAGGGAGAAGGGAGCGGAAAAGTCTCCACCGGACGCGGCCATGGCTCGGGGGGGGGGG
GGCAGCGGAGGAGCGCTTCCGGCCGACGTCTCGTCGCTGATTGGCTTCTTTTCCTCCCGCCGTGTGTGAAA
ACACAAATGGCGTGTTTTGGTTGGCGTAAGGCGCCTGTCAGTTAACGGCAGCCGGAGTGCGCAGCCGCCGG
CAGCCTCGCTCTGCCCACTGGGTGGGGCGGGAGGTAGGTGGGGTGAGGCGAGCTGGACGTGCGGGCGC
GGTCGGCCTCTGGCGGGGCGGGGGAGGGGAGGGAGGGTCAGCGAAAGTAGCTCGCGCGCGAGCGGCC
GCCCACCCTCCCCTTCCTCTGGGGGAGTCGTTTTACCCGCCGCCGGCCGGGCCTCGTCGTCTGATTGGCT
CTCGGGGCCCAGAAAACTGGCCCTTGCCATTGGCTCGTGTTCGTGCAAGTTGAGTCCATCCGCCGGCCAGC
GGGGGCGGCGAGGAGGCGCTCCCAGGTTCCGGCCCTCCCCTCGGCCCCGCGCCGCAGAGTCTGGCCG
CGCGCCCCTGCGCAACGTGGCAGGAAGCGCGCGCTGGGGGCGGGGACGGGCAGTAGGGCTGAGCGGC
TGCGGGGCGGGTGCAAGCACGTTTCCGACTTGAGTTGCCTCAAGAGGGGCGTGCTGAGCCAGACCTCCATC
GCGCACTCCGGGGAGTGGAGGGAAGGAGCGAGGGCTCAGTTGGGCTGTTTTGGAGGCAGGAAGCACTTGC
TCTCCCAAAGTCGCTCTGAGTTGTTATCAGTAAGGGAGCTGCAGTGGAGTAGGCGGGGAGAAGGCCGCACC
CTTCTCCGGAGGGGGGAGGGGAGTGTTGCAATACCTTTCTGGGAGTTCTCTGCTGCCTCCTGGCTTCTGAGG
ACCGCCCTGGGCCTGGGAGAATCCCTTCCCCCTCTTCCCTCGTGATCTGCAACTCCAGTCTTTCTAGCCTTAA
TTAACCGTTTAAACAATTCTGCAGGAATCTAGTTATTAATAGTAATCAATTACGGGGTCATTAGTTCATAGCCCATA
TATGGAGTTCCGCGTTACATAACTTACGGTAAATGGCCCGCCTGGCTGACCGCCCAACGACCCCCGCCCATT
GACGTCAATAATGACGTATGTTCCCATAGTAACGCCAATAGGGACTTTCCATTGACGTCAATGGGTGGAGTATTT
ACGGTAAACTGCCCACTTGGCAGTACATCAAGTGTATCATATGCCAAGTACGCCCCCTATTGACGTCAATGAC
GGTAAATGGCCCGCCTGGCATTATGCCCAGTACATGACCTTATGGGACTTTCCTACTTGGCAGTACATCTACG
TATTAGTCATCGCTATTACCATGGTCGAGGTGAGCCCCACGTTCTGCTTCACTCTCCCCATCTCCCCCCCCTC
CCCACCCCCAATTTTGTATTTATTTATTTTTTAATTATTTTGTGCAGCGATGGGGGCGGGGGGGGGGGGGGGC
GCGCGCCAGGCGGGGCGGGGCGGGGCGAGGGGCGGGGCGGGGCGAGGCGGAAAGGTGCGGCGGCA
GCCAATCARAGCGGCGCGCTCCGAAAGTTTCCTTTTATGGCGAGGCGGCGGCGGCGGCGGCCCTATAAAAA
GCGAAGCGCGCGGCGGGCGGGAGTCGCTGCGCGCTGCCTTCGCCCCGTGCCCCGYTCCGCCGCCGCCT
CGCGCCGCCCGCCCCGGYTCTGACTGACCGCGTTACTCCCACAGGTGAGCGGGCGGGACGGCCCTTCTC
CTCCGGGYTGTAATTAGCGCTTGGTTTAATGACGGYTTGTTTCTTTTCTGTGGYTGCGTGAAAGCCTTGAGGGGC
TCCGGGAGGGCCCTTTGTGCGGGGGGAGCGGCTCGGGGGGTGCGTGCGTGTGTGTGTGCGTGGGGAGCG
CCGCGTGCGGCTCCGCGCTGCCCGGCGGCTGTGAGCGCTGCGGGCGCGGCGCGGGGCTTTGTGCGCTC
CGCAGTGTGCGCGAGGGGAGCGCGGCCGGGGGCGGTGCCCCGCGGTGCGGGGGGGGCTGCGAGGGG
AACAAAGGCTGCGTGCGGGGTGTGTGCGTGGGGGGGTGAGCAGGGGGTGTGGGCGCGTCGGTCGGGCTG
CAACCCCCCCTGCACCCCCCTCCCCGAGTTGCTGAGCACGGCCCGGCTTCGGGTGCGGGGCTCCGTACG
GGGCGTGGCGCGGGGCTCGCCGTGCCGGGCGGGGGGTGGCGGCAGGTGGGGGTGCCGGGCGGGGCG
GGGCCGCCTCGGGCCGGGGAGGGCTCGGGGGAGGGGCGCGGCGGCCCCCGGAGCGCCGGCGGCTGT
CGAGGCGCGGCGAGCCGCAGCCATTGCCTTTTATGGTAATCGTGCGAGAGGGCGCAGGGACTTCCTTTGTC
CCAAATCTGTGCGGAGCCGAAATCTGGGAGGCGCCGCCGCACCCCCTCTAGCGGGCGCGGGGCGAAGC
GGTGCGGCGCCGGCAGGAAGGAAATGGGCGGGGAGGGCCTTCGTGCGTCGCCGCGCCGCCGTCCCCTT
CTCCCTCTCCAGCCTCGGGGCTGTCCGCGGGGGGACGGCTGCCTTCGGGGGGGACGGGGCAGGGCGGG
GTTCGGCTTCTGGCGTGTGACCGGCGGCTCTAGAGCCTCTGCTAACCATGTTCATGCCTTCTTCTTTTTCCTAC
AGCTCCTGGGCAACGTGCTGGTTATTGTGCTGTCTCATCATTTTGGCAAAGAATTGATTTGATACCGCGGGCCC
TAAGAAGTTCCTATTCTCTAGAAAGTATAGGAACTTCGTCGACATTTAAATCATTTAAAT**ATAACTTCGTATAATGT**
ATGCTATACGAAGTTATTCGCGATGAATAAATGAAAGCTTGCAGATCTGCGACTCTAGAGGATCTGCGACTC
TAGAGGATCATAATCAGCCATACCACATTTGTAGAGGTTTTACTTGCTTTAAAAAACCTCCCACACCTCCCC
CTGAACCTGAAACATAAAATGAATGCAATTGTTGTTGTTAACTTGTTTATTGCAGCTTATAATGGTTACAAATA
AAGCAATAGCATCACAAATTTCACAAATAAAGCATTTTTTTCACTGCATTCTAGTTGTGGTTTGTCCAAACTCA
TCAATGTATCTTATCATGTCTGGATCTGCGACTCTAGAGGATCATAATCAGCCATACCACATTTGTAGAGGTT

1314 **TTACTTGCTTTAAAAAACCTCCCACACCTCCCCCTGAACCTGAAACATAAAATGAATGCAATTGTTGTTGTTA**
1315 **ACTTGTTTATTGCAGCTTATAATGGTTACAAATAAAGCAATAGCATCACAAATTTCACAAATAAAGCATTTTTTT**
1316 **CACTGCATTCTAGTTGTGGTTTGTCCAAACTCATCAATGTATCTTATCATGTCTGGATCTGCGACTCTAGAGG**
1317 **ATCATAATCAGCCATACCACATTTGTAGAGGTTTTACTTGCTTTAAAAAACCTCCCACACCTCCCCCTGAAC**
1318 **CTGAAACATAAAATGAATGCAATTGTTGTTGTTAACTTGTTTATTGCAGCTTATAATGGTTACAAATAAAGCAAT**
1319 **AGCATCACAAATTTCACAAATAAAGCATTTTTTTCACTGCATTCTAGTTGTGGTTTGTCCAAACTCATCAATGT**
1320 **ATCTTATCATGTCTGGATCCCCATCAAGCTGATCCGGAACCCTTAATATAACTTCGTATAATGTATGCTATAC**
1321 **GAAGTTAT**TAGGTCCCTCGACCTGCAGCCCAAGCTAGATCGAATTCGGCCGGCCTTGTACGCGTGCCACC**A**
1322 **TGGGCAAGCCCATCCCCAACCCCCTGCTGGGCCTGGACAGCACC**GCTAGC**AAAGACAATACTGTGCCT**
1323 **CTGAAGCTGATCGCTCTCCTGGCTAATGGCGAGTTCCATAGTGGCGAACAGCTGGGAGAAACCCTGGGC**
1324 **ATGTCCAGGGCCGCTATCAACAAGCACATTCAGACTCTGCGCGACTGGGGCGTGGACGTGTTCACCGTG**
1325 **CCCGGAAAGGGCTACTCTCTGCCCGAGCCTATCCCGCTGCTGAACGCTAAACAGATTCTGGGACAGCTG**
1326 **GACGGCGGGAGCGTGGCAGTCCTGCCTGTGGTCGACTCCACCAATCAGTACCTGCTGGATCGAATCGGC**
1327 **GAGCTGAAGAGTGGGGATGCTTGCATTGCAGAATATCAGCAGGCAGGGAGAGGAAGCAGAGGGAGGAAA**
1328 **TGGTTCTCTCCTTTTGGAGCTAACCTGTACCTGAGTATGTTTTGGCGCCTGAAGCGGGGACCAGCAGCAAT**
1329 **CGGCCTGGGCCCGGTCATCGGAATTGTCATGGCAGAAGCGCTGCGAAAGCTGGGAGCAGACAAGGTGC**
1330 **GAGTCAAATGGCCCAATGACCTGTATCTGCAGGATAGAAAGCTGGCAGGCATCCTGGTGGAGCTGGCCG**
1331 **GAATAACAGGCGATGCTGCACAGATCGTCATTGGCGCCGGGATTAACGTGGCTATGAGGCGCGTGGAGG**
1332 **AAAGCGTGGTCAATCAGGGCTGGATCACACTGCAGGAAGCAGGGATTAACCTGGACAGGAATACTCTGG**
1333 **CCGCTACGCTGATCCGAGAGCTGCGGGCAGCCCTGGAACTGTTCGAGCAGGAAGGCCTGGCTCCATAT**
1334 **CTGCCACGGTGGGAGAAGCTGGATAACTTCATCAATAGACCCGTGAAGCTGATCATTGGGGACAAAGAGA**
1335 **TTTTCGGGATTAGCCGGGGGATTGATAAACAGGGAGCCCTGCTGCTGGAACAGGACGGAGTTATCAAACC**
1336 **CTGGATGGGCGGAGAAATCAGTCTGCGGTCTGCCGAAAAG**TAAACGCGTACAAGGCCGGCCCTGCAGGA
1337 ATTCGATATCAAGCTTATCGAT**AATCAACCTCTGGATTACAAAATTTGTGAAAGATTGACTGGTATTCTTAACTA**
1338 **TGTTGCTCCTTTTACGCTATGTGGATACGCTGCTTTAATGCCTTTGTATCATGCTATTGCTTCCCGTATGGCTT**
1339 **TCATTTTCTCCTCCTTGTATAAATCCTGGTTGCTGTCTCTTTATGAGGAGTTGTGGCCCGTTGTCAGGCAACG**
1340 **TGGCGTGGTGTGCACTGTGTTTGCTGACGCAACCCCCACTGGTTGGGGCATTGCCACCACCTGTCAGCTC**
1341 **CTTTCCGGGACTTTCGCTTTCCCCCTCCCTATTGCCACGGCGGAACTCATCGCCGCCTGCCTTGCCCGCT**
1342 **GCTGGACAGGGGCTCGGCTGTTGGGCACTGACAATTCCGTGGTGTTGTCGGGGAAATCATCGTCCTTTCC**
1343 **TTGGCTGCTCGCCTGTGTTGCCACCTGGATTCTGCGCGGGACGTCCTTCTGCTACGTCCCTTCGGCCCTC**
1344 **AATCCAGCGGACCTTCCTTCCCGCGGCCTGCTGCCGGCTCTGCGGCCTCTTCCGCGTCTTCGCCTTCGC**
1345 **CCTCAGACGAGTCGGATCTCCCTTTGGGCCGCCTCCCCGC**ATCGATACCGTCGACCTCGACCTCGACTGT
1346 GCCTTCTAGTTGCCAGCCATCTGTTGTTTGCCCCTCCCCCGTGCCTTCCTTGACCCTGGAAGGTGCCACTCC
1347 CACTGTCCTTTCCTAATAAAATGAGGAAATTGCATCGCATTGTCTGAGTAGGTGTCATTCTATTCTGGGGGGTGG
1348 GGTGGGGCAGGACAGCAAGGGGGAGGATTGGGAAGACAATGGCAGGCATGCTGGGGAACTAGTGGTGCCA
1349 GGGCGTGCCCTTGGGCTCCCCGGCGCGCCGGCTAGAAGATGGGCGGGAGTCTTCTGGGCAGGCTTAAAG
1350 GCTAACCTGGTGTGTGGGCGTTGTCCTGCAGGGGAATTGAACAGGTGTAAAATTGGAGGGACAAGACTTCCC
1351 ACAGATTTTCGGTTTTGTCGGGAAGTTTTTTAATAGGGGCAAATAAGGAAAATGGGAGGATAGGTAGTCATCTGG
1352 GGTTTTATGCAGCAAAACTACAGGTTATTATTGCTTGTGATCCGCCTCGGAGTATTTTCCATCGAGGTAGATTAAA
1353 GACATGCTCACCCGAGTTTTATACTCTCCTGCTTGAGATCCTTACTACAGTATGAAATTACAGTGTCGCGAGTTA
1354 GACTATGTAAGCAGAATTTTAATCATTTTTAAAGAGCCCAGTACTTCATATCCATTTCTCCCGCTCCTTCTGCAGC
1355 CTTATCAAAAGGTATTTTAGAACACTCATTTTAGCCCCATTTTCATTTATTATACTGGCTTATCCAACCCCTAGACA
1356 GAGCATTGGCATTTTCCCTTTCCTGATCTTAGAAGTCTGATGACTCATGAAACCAGACAGATTAGTTACATACAC
1357 CACAAATCGAGGCTGTAGCTGGGGCCTCAACACTGCAGTTCTTTTATAACTCCTTAGTACACTTTTTGTTGATCC
1358 TTTGCCTTGATCCTTAATTTTCAGTGTCTATCACCTCTCCCGTCAGGTGGTGTTCCACATTTGGGCCTATTCTCAG
1359 TCCAGGGAGTTTTACAACAATAGATGTATTGAGAATCCAACCTAAAGCTTAACTTTCCACTCCCATGAATGCCTC
1360 TCTCCTTTTTCTCCATTTATAAACTGAGCTATTAACCATTAATGGTTTCCAGGTGGATGTCTCCTCCCCCAATATTA
1361 CCTGATGTATCTTACATATTGCCAGGCTGATATTTTAAGACATTAAAAGGTATATTTCATTATTGAGCCACATGGTA
1362 TTGATTACTGCTTACTAAAATTTTGTCATTGTACACATCTGTAAAAGGTGGTTCCTTTTGGAATGCAAAGTTCAGGT
1363 GTTTGTTGTCTTTCCTGACCTAAGGTCTTGTGAGCTTGTATTTTTTCTATTTAAGCAGTGCTTTCTCTTGGACTGGCT

TGACTCATGGCATTCTACACGTTATTGCTGGTCTAAATGTGATTTTGCCAAGCTTCTTCAGGACCTATAATTTTGC
TTGACTTGTAGCCAAACACAAGTAAAATGATTAAGCAACAAATGTATTTGTGAAGCTTGGTTTTTAGGTTGTTGTGT
TGTGTGTGCTTGTGCTCTATAATAATACTATCCAGGGGCTGGAGAGGTGGCTCGGAGTTCAAGAGCACAGACT
GCTCTTCCAGAAGTCCTGAGTTCAATTCCCAGCAACCACATGGTGGCTCACAACCATCTGTAATGGGATCTGA
TGCCCTCTTCTGGTGTGTCTGAAGACCACAAGTGTATTCACATTAAATAAATAAATCCTCCTTCTTCTTTTTTTT
TTTTTTAAAGAGAATACTGTCTCCAGTAGAATTTACTGAAGTAATGAAATACTTTGTGTTTGTTCCAATATGGTAGCC
AATAATCAAATTACTCTTTAAGCACTGGAAATGTTACCAAGGAACTAATTTTTATTTGAAGTGTAACTGTGGACAGA
GGAGCCATAACTGCAGACTTGTGGGATACAGAAGACCAATGCAGACTTTAATGTCTTTTCTCTTACACTAAGCA
ATAAAGAAATAAAAATTGAACTTCTAGTATCCTATTTGTTTAAACTGCTAGCTTTACTTAACTTTTGTGCTTCATCTAT
ACAAAGCTGAAAGCTAAGTCTGCAGCCATTACTAAACATGAAAGCAAGTAATGATAATTTTGGATTTCAAAAATGT
AGGGCCAGAGTTTAGCCAGCCAGTGGTGGTGCTTGCCTTTATGCCTTTAATCCCAGCACTCTGGAGGCAGAG
ACAGGCAGATCTCTGAGTTTGAGCCCAGCCTGGTCTACACATCAAGTTCTATCTAGGATAGCCAGGAATACAC
ACAGAAACCCTGTTGGGGAGGGGGGCTCTGAGATTTCATAAAATTATAATTGAAGCATTCCCTAATGAGCCACT
ATGGATGTGGCTAAATCCGTCTACCTTTCTGATGAGATTTGGGTATTATTTTTTCTGTCTCTGCTGTTGGTTGGGTC
TTTTGACACTGTGGGCTTTCTTTAAAGCCTCCTTCCTGCCATGTGGTCTCTTGTTTGCTACTAACTTCCCATGGCT
TAAATGGCATGGCTTTTTGCCTTCTAAGGGCAGCTGCTGAGATTTGCAGCCTGATTTCCAGGGTGGGGTTGGG
AAATCTTTCAAACACTAAAATTGTCCTTTAATTTTTTTTTTAAAAAATGGGTTATATAATAAACCTCATAAAATAGTTAT
GAGGAGTGAGGTGGACTAATATTAAATGAGTCCCTCCCCTATAAAAGAGCTATTAAGGCTTTTTGTCTTATACTTA
ACTTTTTTTTTAAATGTGGTATCTTTAGAACCAAGGGTCTTAGAGTTTTAGTATACAGAAACTGTTGCATCGCTTAAT
CAGATTTTCTAGTTTCAAATCCAGAGAATCCAAATTCTTCACAGCCAAAGTCAAATTAAGAATTTCTGACTTTTAAT
GTTAATTTGCTTACTGTGAATATAAAAATGATAGCTTTTCCTGAGGCAGGGTCTCACTATGTATCTCTGCCTGATC
TGCAACAAGATATGTAGACTAAAGTTCTGCCTGCTTTTGTCTCCTGAATACTAAGGTTAAAATGTAGTAATACTTTT
GGAACTTGCAGGTCAGATTCTTTTATAGGGGACACACTAAGGGAGCTTGGGTGATAGTTGGTAAAATGTGTTTCA
AGTGATGAAAACTTGAATTATTATCACCGCAACCTACTTTTTAAAAAAAAAAGCCAGGCCTGTTAGAGCATGCTTA
AGGGATCCCTAGGACTTGCTGAGCACACAAGAGTAGTTACTTGGCAGGCTCCTGGTGAGAGCATATTTCAAAA
AACAAGGCAGACAACCAAGAAACTACAGTTAAGGTTACCTGTCTTTAAACCATCTGCATATACACAGGGATATT
AAAATATTCCAAATAATATTTCATTCAAGTTTTCCCCCATCAAATTGGGACATGGATTTCTCCGGTGAATAGGCAG
AGTTGGAAACTAAACAAATGTTGGTTTTGTGATTTGTGAAATTGTTTTCAAGTGATAGTTAAAGCCCATGAGATACA
GAACAAAGCTGCTATTTCGAGGTCTCTTGGTTTATACTCAGAAGCACTTCTTTGGGTTTCCCTGCACTATCCTGA
TCATGTGCTAGGCCTACCTTAGGCTGATTGTTGTTCAAATAAACTTAAGTTTCCTGTCAGGTGATGTCATATGATTT
CATATATCAAGGCAAAACATGTTATATATGTTAAACATTTGTACTTAATGTGAAAGTTAGGTCTTTGTGGGTTTGATT
TTTAATTTTCAAAACCTGAGCTAAATAAGTCATTTTTACATGTCTTACATTTGGTGGAATTGTATAATTGTGGTTTGCA
GGCAAGACTCTCTGACCTAGTAACCCTACCTATAGAGCACTTTGCTGGGTCACAAGTCTAGGAGTCAAGCATT
TCACCTTGAAGTTGAGACGTTTTGTTAGTGTATACTAGTTTATATGTTGGAGGACATGTTTATCCAGAAGATATTCA
GGACTATTTTTGACTGGGCTAAGGAATTGATTCTGATTAGCACTGTTAGTGAGCATTGAGTGGCCTTTAGGCTTG
AATTGGAGTCACTTGTATATCTCAAATAATGCTGGCCTTTTTTAAAAAGCCCTTGTTCTTTATCACCCTGTTTTCTA
CATAATTTTTGTTCAAAGAAATACTTGTTTGGATCTCCTTTTGACAACAATAGCATGTTTTCAAGCCATATTTTTTTTC
CTTTTTTTTTTTTTTTTTGGTTTTTCGAGACAGGGTTTCTCTGTATAGCCCTGGCTGTCCTGGAACTCACTTTGTAGA
CCAGGCTGGCCTCGAACTCAGAAATCCGCCTGCCTCTGCCTCCTGAGTGCCGGGATTAAAGGCGTGCACCA
CCACGCCTGGCTAAGTTGGATATTTTGTTATATAACTATAACCAATACTAACTCCACTGGGTGGATTTTTAATTCA
GTCAGTAGTCTTAAGTGGTCTTTATTGGCCCTTCATTAAAATCTACTGTTCACTCTAACAGAGGCTGTTGGTACTA
GTGGCACTTAAGCAACTTCCTACGGATATACTAGCAGATTAAGGGTCAGGGATAGAAACTAGTCTAGCGTTTTG
TATACCTACCAGCTTTATACTACCTTGTTCTGATAGAAATATTTCAGGACATCTAGagtgtactataaggttgatggtaagctt
ataaggaacttgaaagtggagtaactactccatttctctgaggggagaattaaaatttttgaccaagtgttgttgagccactgagaatggtctcagaa
cataacttcttaaggaaccttcccagattgccctcaacactgcaccacatttggtcctgcttgaacattgccatggctcttaaagtcttaattaagaa
tattaattgtgtaattattgtttttcctcctttagatcattccttgaggacaggacagtgcttgtttaaggctatatttctgctgtctgagcagcaacaggtc
ttcgagatcaacatgatgttcat-3’

SMethods, Sequence. Ai14-TurboID_Rosa26 HDR fragment and sequence annotations.

1413 **SMethods, Table. Primer sequence and fragment size information**

1414

1415

Name	ID	Sequence (5' → 3')	mer	Orientation	Target Region	Fragment Size
Rosa26 Left Arm	29194	CGCCTAAAGAAGAGGCTGTG	20	Sense	Upstream ROSA26 left-arm	1295 bp
	7604	CGCGGAACTCCATATATGGGCT	22	Anti-sense	5'-End-CAG-promoter	
Rosa26 Right Arm	2736	GCAGGACAGCAAGGGGGAGGAT	22	Sense	bGH poly(A) signal	4736 bp
	36502	GACCTGTTGCTGCTCAGACAGC	22	Anti-sense	Downstream Rosa26 right arm	
Diagnostic Routine Genotyping PCR	14025	CTCTGCTGCCTCCTGGCTTCT	21	Sense	ROSA26 upstream insertion site	146 bp
	24229	CGCCCACACACCAGGTTAG	19	Anti-sense	ROSA26 downstream insertion site	
	30545	AAGCTGATCCGGAACCCTTAA	21	Sense	Upstream loxP2	254 bp (WT) 370 bp (Cre)
	26512	CTACAGCTCCTGGGCAACG	19	Sense	upstream loxP1 (3'-End CAG promoter)	
	38281	CCAGGGTTTCTCCCAGCTGT	20	Anti-sense	TurboID	

1416

1417

1418

1419

1420